Nano Research Energy

ISSN 2791-0091 (print); 2790-8119 (online)
https://doi.org/10.26599/NRE.2023.9120080

Review Article

Property modulations of two-dimensional materials under compression

Zhen Wu, Yuxi Wang, Yunjie Dou, Lin Zhou, and Jia Zhu (✉)

National Laboratory of Solid State Microstructures, College of Engineering and Applied Sciences and Jiangsu Key Laboratory of Artificial Functional Materials, Nanjing University, Nanjing 210093, China

Received: 20 February 2023 / **Revised:** 19 April 2023 / **Accepted:** 8 May 2023

ABSTRACT

Two-dimensional (2D) materials have attracted considerable research interest, leading to significant advances in energy applications in recent years, such as lithium batteries, catalysis, electronics, and thermoelectrics, owing to their rich controllable properties and excellent performances. Recently, pressure has been successfully employed as an effective method for property modulation of 2D materials, through tuning electronic orbitals and bonding patterns. In this review, we summarize recent progresses in the pressure-driven property modulations and elucidate the underlying mechanism of the pressure modulation of 2D materials. Further, we identify the remaining challenges and opportunities in this new, vibrant area of research for energy conversion and utilization. Among the different property modulation strategies, the *in situ* application of high pressure is systematically identified as a promising knob for 2D materials. This review is expected to inspire further research on the fundamental understanding and practical applications of high-pressure modulation in 2D materials.

KEYWORDS

two-dimensional material, property modulations, hydrostatic pressure, diamond anvil cell, energy applications

1 Introduction

Two-dimensional (2D) materials have attracted widespread research interest since the discovery of mechanically exfoliated graphene owing to their abundance and unique properties [1]. Each layer in a 2D material is composed of covalent bonds connecting the in-plane atoms, while the weak van der Waals (vdW) force maintains the interlayer structures. The properties of 2D materials are closely related to the electron interaction and spin-orbit coupling between vdW layers; therefore, structural modulation is essential for tuning the properties of 2D materials and expanding their applications [2–7].

Several factors can modulate the physical properties of materials, such as pressure, temperature, electromagnetic field, magnetic field, and doping. Research on high-pressure techniques has considerably advanced over the last decade owing to the synergistic development of probing technology and various pressure devices, particularly diamond anvil cells (DACs) [8]. The DAC, mainly composed of two opposing diamonds, is a unique apparatus capable of generating a static pressure of up to hundreds of GPa and realizing a full range of *in situ* measurements owing to transparent windows allowing optical access [9]. Developments in microfabrication and nanotechnology have promoted considerable progress in high-pressure technology, enabling the *in situ* observation of variations in the electrical, thermal, and even thermoelectric properties of DAC devices. The application of high pressure can alter the interlayer interaction and electron density of 2D materials, thereby modulating crystal and band structures and even phase transitions; therefore, it can regulate the physical properties and advanced applications of target materials [10, 11].

In this review, we summarize recent progresses in the pressure-driven property modulations of 2D materials and expound promising applications in the energy field [12]. Owing to their weak interlayer vdW forces, 2D materials can be more efficiently compressed than their three-dimensional counterparts with covalent or ionic bonds and may even exhibit new properties owing to phase transitions (Fig. 1). Therefore, applying high pressure can effectively regulate energy bands, thereby establishing a relationship between structures and high pressure. The effects of high-pressure modulation on the properties of optics, electrics, thermotics, and magnetics of 2D materials can be investigated owing to their tunable band gap and crystal structures. These modulations can be further investigated in energy transport and conversion, which can expand the applications of target materials in energy field. Moreover, as a new dimension, introducing high-pressure science is expected to open new avenues for 2D materials research and provide more possibilities for various applications.

Address correspondence to Jia Zhu, jiazhu@nju.edu.cn

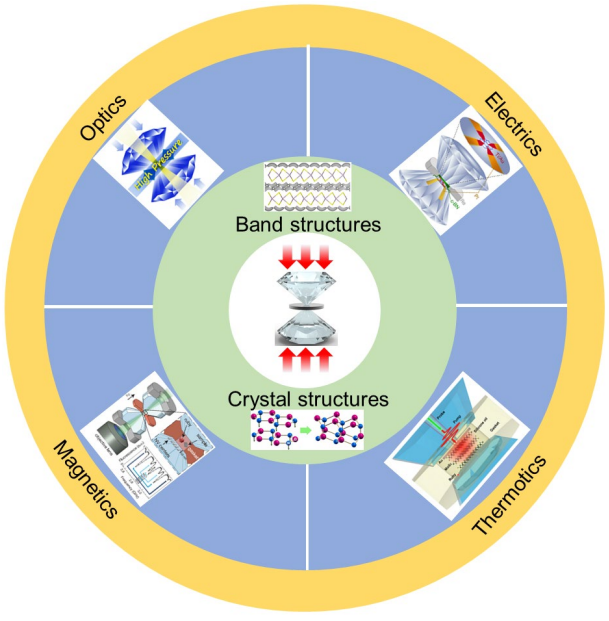

Figure 1 The pressure-induced modulations of the physical properties in 2D materials.

2 Crystal and band structure modulations

Pressure is a powerful variable that can tune structural parameters, including the atomic position, periodicity, symmetry, coordination, and ordering in crystalline or amorphous materials. Through atomic structure rearrangement, unusual phase transitions can be achieved, and materials that are difficult to synthesize under ordinary conditions can be obtained. The recent progress in the manipulation of 2D crystals enables the study of the physical and chemical properties of 2D materials under pressure.

2.1 2D heterostructures

Layered vdW materials possess unique properties owing to their in-plane covalent bonds and weak interlayer interactions. Crystal and electronic band structures are often tuned by strain and layer spacing, which can further dominate the performance of 2D-material-based electronic and optoelectronic devices. Zeng et al. reported a sphere diameter engineering technique to manipulate the bandgap of 2D MoS_2 [13]. Bai et al. presented the strain-induced one-dimensional moiré patterns along with photoluminescence measurements of the corresponding excitonic emission from $WSe_2/MoSe_2$ heterobilayers [14].

Because of the weaker interlayer interactions of two-dimensional materials, the interlayer distance is easily compressed under pressure, leading to the band engineering. In a heterobilayer with weak interlayer interaction, band alignment is difficult to observe due to the weak interlayer coupling, in which interfacial contamination or a large interlayer distance severely suppresses the coupling [15, 16]. Xia et al. used a designed two-step CVD process and fabricated WSe_2-$MoSe_2$ heterostructures with precise 2H stacking [17]. By induced hydrostatic pressure, they tuned the interlayer distance and therefore the band structure. The change in interlayer exciton behavior was observed at approximately 1.0 GPa (~4% volume change) with the two ambient-pressure excitonic transitions replaced by two new ones that also exhibit distinct pressure responses, which revealed a pressure-induced transition in the band structure of the heterostructures (Fig. 2(a)). Through the compression, it was superior as a continuous and reversible tuning method, compared with most of the straining techniques, in which only limited changes could be achieved in the lattice parameters. It hindered the effective modulations of properties in vdW heterostructures, for example, less than 2% volume change through strain engineering, or ~5% shortening in interlayer distance by using traditional piston-cylinder setup [18–21].

2.2 2D perovskites

Recently 2D organic-inorganic Ruddlesden-Popper perovskites with layered structures are considered as promising candidates for future nanophotonics and optoelectronics [22–24]. The hybrid nature and soft lattice of these materials make their crystal and band structures susceptible to external driving forces, such as pressure and temperature, which are significantly different from conventional semiconductors under stress [25]. On this occasion, research on the compressibility of 2D perovskites becomes increasingly attractive due to the anisotropy of 2D perovskites and the combination of two soft organic and inorganic sublattices, which may lead to unusual phenomena [26, 27]. Depending on the direction of the applying pressure, the crystal lattice will distort, leading to the octahedral tilting and directional bond contraction, while the organic layers can serve as buffers to release the excess compression [28].

As shown in Fig. 2(b), 2D perovskite $(PEA)_2PbI_4$ (PEA = phenylethylamine) was loaded into a DAC to systematically investigate its optical and structural behaviors under pressure. Ultrabroad tunable emission has been observed, showing 320 meV tunability at 0 to 3.5 GPa. It is broader than the bulk $MAPbX_3$ bandgap tunability, which is generally less than 80 meV [29–31]. The long-chain PEA molecules and 2D configuration play a key role in modulating the lattice and band structures. Similarly, Liu et al. reported metastable states of 2D $(BA)_2(MA)_2Pb_3I_{10}$ ($CH_3(CH_2)_3NH_3^+$, (BA); $CH_3NH_3^+$, (MA)) reached through structural amorphization under compression followed by recrystallization via decompression and achieved a long-term large bandgap narrowing, 8.2% after a loop from 26 GPa to ambient pressure [28]. Fang et al. observed the appearance of pressure-induced emission (PIE) at 2.5 GPa. Upon further compression at 25 GPa, the band gap narrowed by about 16% (2.61 to 2.19 eV) accompanied by a color variance from light yellow to dark yellow [32]. In other similar 2D perovskites, changes in bandgap were also observed by the PL spectra with increasing pressure [33, 34]. Another type of lead-free inorganic perovskite compound, 2D $Cs_3Sb_2I_9$, is severely hindered by the large band gap. The band gap was narrowed from 2.05 to 1.36 eV under compression in a DAC without any structural transformation. Therefore, it is an effective way to achieve the band gap modulation, which meets the demand of approaching the Shockley-Queisser limit. Besides, Kong et al. demonstrated their irreversible behavior influenced by the compression, which suggested that pressure/strain engineering could viably modulate the structures more than *in situ*, thus potentially fostering the development of light-emitting materials and optoelectronic devices [35].

2.3 2D TMDs

The large reversible bandgap modulation of semiconducting MoS_2, which can be realized by *in situ* high pressure, is attractive for highly tunable optoelectronics, nanoelectronics, and flexible electronics. It can enable new opportunities based on the dynamic

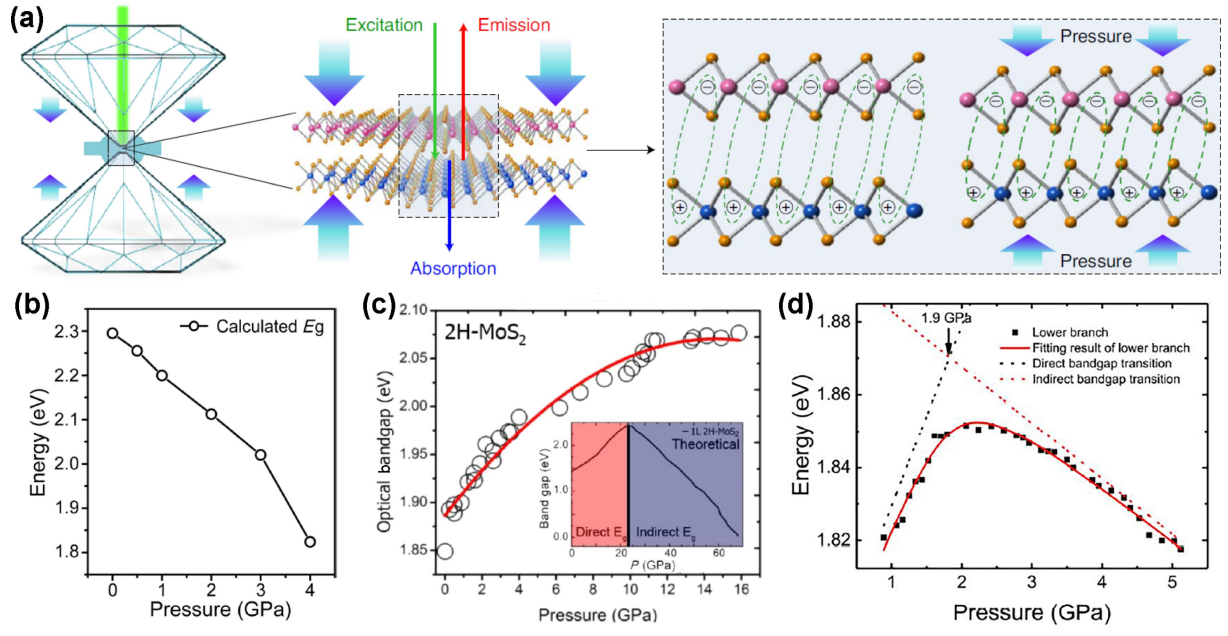

Figure 2 (a) Schematic illustration of band engineering of the interlayer excitonic states in 2D vdW heterostructures by using hydrostatic pressure through a DAC. Reproduced with permission from Ref. [17], © The Author(s), under exclusive licence to Springer Nature Limited 2020. (b) The band gap evolution with increasing pressure. Reproduced with permission from Ref. [25], © American Association for the Advancement of Science 2019. (c) Derived band gap at high pressures. Extracted from the Lorentzian fit from the PL peaks, the band gap is shown to increase as a function of pressure. Reproduced with permission from Ref. [36], © American Chemical Society 2015. (d) The energy evolution of the predominant PL peak versus pressure. Black dots represent peak energies of monolayer MoS_2 under various pressures, taken as the lower branch; red solid line represents the fitting result of the lower branch; and black and red dotted lines represent the direct and indirect transition under various pressures extracted from the fitting, respectively. Reproduced with permission from Ref. [38], © American Association for the Advancement of Science 2017.

strong electron-phonon coupling. As shown in Fig. 2(c), Nayak et al. investigated the electronic structure of monolayer 2H-MoS_2 via DAC and density functional theory (DFT) calculations [36]. The direct optical band gap of the monolayer sample tested by PL increased from 1.85 to 2.08 eV with the hydrostatic pressure due to absence of interlayer interactions. The lattice vibrations detected by Raman spectroscopy revealed key changes occurring to the crystal lattice at high pressures, which induced a blue shift (phonon hardening) in MoS_2 [37]. It is important for the study on probing the intrinsic response of the strain-property relations in a controlled environment. The insights provided by this study can guide practical realization of strained MoS_2 devices. Further on, Fu et al. confirmed the bandgap transition of direct-to-indirect through the PL spectra of monolayer MoS_2 under hydrostatic pressure in DAC at room temperature [38]. It is well-known that the band structure of monolayer MoS_2 has a direct gap at the K point, and the second lowest conduction band minimum is located at the L point. It may interact with the valence band maximum to make an indirect optical bandgap transition. With the increasing hydrostatic pressure, the energy peak primarily appeared as a blue shift below 1.9 GPa and then a redshift. Combining with first-principle calculations, the transition was demonstrated to originate from the change from K to L valley of the conduction band minimum (Fig. 2(d)). For the bilayer MoS_2 with the VBM located at L point, Dou et al. demonstrated a direct K-K to an indirect ΛK interband transition by tuning the hydrostatic pressure of approximately 1.5 GPa [39]. On this basis, they found that the valence band maximum of the monolayer MoS_2 splitting at the K point, induced by spin-orbit coupling, remained almost unchanged with increasing pressure up to 3.98 GPa, which indicated the insensitive spin-orbit coupling to the pressure. However, for bilayer and trilayer MoS_2, the splitting shows an increasing trend with increasing pressure because of the pressure-induced strengthening of interlayer coupling [40]. Chi et al. observed a new 2Ha phase at high pressures through the first-order phase transformation of the initial 2Hc phase through synchrotron X-ray diffraction and Raman scattering measurements, which involves a change in interlayer interactions and bonding. The metallic state was obtained in 2Ha phase after the phase transformation was complete at 40 GPa. Riflikova et al. predicted a similar phenomenon for the layered semiconductors 2Hc-$MoSe_2$ and 2Hc-$MoTe_2$ undergoing metallization at higher pressures, based on first-principles calculations [41, 42].

2.4 Graphene

Although the Raman spectra of silicon remained characteristically unchanged under pressure, the effect of a substrate could not be entirely neglected for the monolayer located on the Si/SiO_2 wafer. In recent years, graphene-based nanodevices developed rapidly and were considered a potential candidate in high-speed electronic devices, for high carrier mobility and flexibility. However, the gapless character of graphene limited the application. For bilayer graphene, the largest bandgap obtained so far was several hundred meV, and it is still far below the practical application threshold. Ke et al. transferred trilayer graphene onto a diamond surface using a polydimethylsiloxane (PDMS) stamping technique, with high-resolution microscopy and Raman spectra measurements adopted to confirm the sample quality during the transfer process [43]. A semimetal-to-semiconductor transition was observed with the increasing pressure and the 2.5 ± 0.3 eV bandgap was obtained in this compressed Bernal-stacked trilayer graphene by modulating the interlayer interaction, through systematic electrical and absorption measurements. Besides, Nicolle et al. reported a phase transition under hydrostatic compression for the trilayer sample, probably because of the formation of silanol groups on the SiO_2 substrate [44].

2.5 Other 2D materials

For the other 2D materials, like few-layered g-C_3N_4, Hu et al. demonstrated that the strengthening of pressure-induced interlayer interactions influenced the charge separation of a photon-generated carrier, thus leading to a PL enhancement. They emphasized the interlayer interactions as a dominant role for PL engineering under compression, caused by the interlayer pressure [45]. Xiang showed a suppressing band gap in the elemental semiconductor black phosphorus induced by hydrostatic pressure and an electronic topological transition took place at about 1.2 GPa, as well as the Bi_2Te_3, evidenced by Polian et al. [46, 47].

3 Optical modulations

3.1 2D perovskite

Due to the changes in crystal and energy band structures under pressure, electronic and excitonic structures are also extensively altered in 2D samples using DAC. For example, changes in lattice and band structures always lead to the rearrangement of the electron clouds, thus modulating basic optical properties. As shown in Fig. 3(a), a 2D perovskite microplate of [$(PEA)_2PbI_4$] was exfoliated from a high-quality single crystal with highly oriented layer structure and sealed in symmetric DAC with hydrostatic pressure [25]. With the increasing pressure, the fluorescence of the nanoplate gradually changes from green to red, as shown in microscopic images at the same lamp power. Below 3.5 GPa, the color could recover to the beginning with the gradually released pressure. However, over 3.5 GPa, the fluorescence quenched and lost the reversibility. Similar color changes are common in 2D perovskites, caused by the shortening of interlayer spacing and the effect of changes in band structure through the increasing pressure [48–50].

3.2 Graphene

Because of the manipulated pressure, the materials can shorten the interlayer spacing and further form covalent bonds instead of van der Waals interaction. For the typical 2D materials graphene, Ke et al. demonstrated that trilayer and few-layer graphene gradually became transparent with the increasing pressure by the optical microscopy observations. The pressure-induced sp^2-sp^3 diamondization transition from mechanically exfoliated few-layer graphene to a pristine diamane was realized via compression. Naturally, the large band gap (about 2.8 eV) of the atomically thin diamond led to the transparency under high pressure [51]. It provided a method for the successful synthesis of pristine

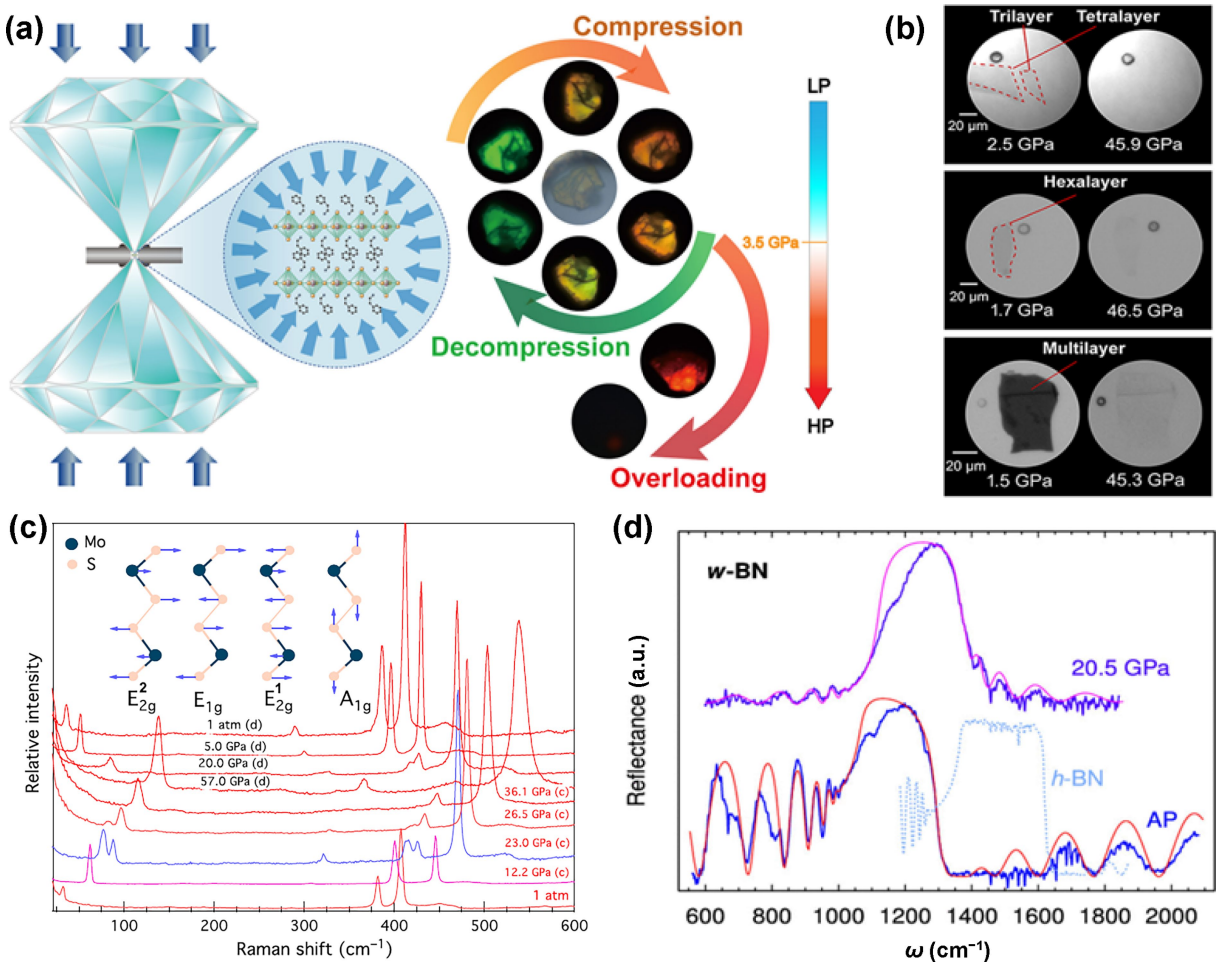

Figure 3 (a) Schematics of the experiment and optical emission behavior of the 2D perovskite $(PEA)_2PbI_4$ under high pressure. Reproduced with permission from Ref. [25], © American Association for the Advancement of Science 2019. (b) Optical microscopy images of compressed tri-, tetra-, hexa-, and multilayer graphene (graphite) samples in transmission mode with a white light source. Reproduced with permission from Ref. [51], © American Chemical Society 2020. (c) Raman spectra of MoS_2 at various pressures up to 57 GPa in both the compression and decompression run. Reproduced with permission from Ref. [56], © American Physical Society 2014. (d) Reflectance spectra at normal incidence of w-BN at 20.5 GPa and of the cold-pressed w-BN sample at ambient pressure outside the DAC. Reproduced with permission from Ref. [74], © American Chemical Society 2019.

diamane, which attracted the research interest due to its unique physical, chemical, and mechanical properties. Similar optical transparency conversion was also realized in the trilayer graphene, which covered the transition from semimetal to semiconductor by applying pressure. For further research, *in situ* high-pressure Raman spectroscopy was used to study graphene with different layers, and the redshift of the G band was always observed with increasing pressure, either freestanding or on the Si/SiO_2 and Cu substrate, which was predicted by the structural transition under compression [52–55].

3.3 2D TMDs

As one of the most widely studied 2D materials, property modulations of TMDs via compression attracted a lot of research interest in recent years. As shown in Fig. 3(c), Chi et al. demonstrated a structural transition between 20 and 30 GPa through *in situ* Raman spectroscopy [56]. The splitting of the E^1_{2g} at 19.1 GPa was considered as experimental evidence for the presence of the new 2Ha phase due to the layer sliding, which was also reported in other studies [57–59]. Both the intralayer phonon mode E_{2g} and the interlayer phonon mode A_{1g} observed a red shift under compression, similar to the graphene. Usually, in the high-pressure study performed on a sample characterized by Raman spectroscopy, the Raman shift is plotted as a function of pressure under hydrostatic stress. However, for ultra-thin 2D materials, different substrates and transfer media present prominent effects on the slope of this function [60]. Besides the hydrostatic pressure in DAC, Zhuang et al. studied the pressure-induced transformations of MoS_2 under non-hydrostatic conditions. The metallization was both observed under these two conditions at 17 GPa and 20 GPa, and it was irreversible only under non-hydrostatic pressure [61]. On this basis, Zhao et al. further investigated the pressure-induced behavior of $MoSe_2$ up to 60 GPa and found that the $MoSe_2$ was completely different from the MoS_2, evolving from an anisotropic 2D layered network to a 3D structure without a structural transition. The changes of measured synchrotron IR spectra via compression were consistent with the large electronic evolution of $MoSe_2$, band-gap narrowing followed by metallization [62].

3.4 2D BN

2D h-BN is consistent by the intralayer covalent bonds, bonded by the boron and nitrogen atoms, and the interlayer vdW force. It exhibits similar intralayer lattice constants and interlayer distances (3.30–3.33 Å), compared with the graphene [63, 64]. 2D BN material has attracted enormous research interest because of its unique electronic and thermal conductivity properties and has thus been extensively studied as the gate dielectric [65], electrical packaging [66, 67] and tunneling junction [68, 69] due to the defect-free, ultra-flat nature and large band gap (above 5.9 eV). It can also be observed phase transition and band modulations owing to the shortening of interlayer spacing under compression, which is similar to the graphene. Based on the previous theoretical calculations [70–72], Meng et al. firstly reported the observation of the conversion process of sp^2- and p-bonding to sp^3 bonding, by probing the boron and nitrogen near K-edge spectroscopy using inelastic X-ray scattering [73]. On this basis, Segura et al. presented the optical spectrum of the pressure-induced phase transition from h-BN to w-BN, with an infrared reflectance and transmission study. The phase transition is nonreversible and is completed at about 13 GPa. The reflectance spectrum is shown in Fig. 3(d), which shows the reflectance spectrum at normal incidence of the w-BN sample at 20.5 GPa, as well as the distinct spectrum of the h-BN displaying at higher frequencies, for comparison [74]. These results demonstrated that the pressure-induced phase transition from h-BN to w-BN was not reversible upon pressure release after the stabilization of the wurtzite phase at high pressure, which was contrary to the prior suggestion reported by Saha et al. in 2006 [75]. Besides, dielectric properties of w-BN were investigated by fitting a reflectivity model, in consideration of the contribution of the polar modes. Maybe defects introduced during the pressurization process resulted in the higher damping and the loss of uniformity in the reflectivity across the reststrahlen band.

3.5 2D wurtzite-type materials

Besides, optical studies of other wurtzite-type semiconductors were also carried out by applying high pressure. For example, Xia et al. demonstrated a pressure-induced first-order phase transition of gallium nitride from the wurtzite structure to the rocksalt structure at the pressure of 37 GPa [76]. Marjon et al. investigated Raman spectra of aluminum nitride under compression, which had been measured up to 25 GPa, and observed the wurtzite-to-rocksalt phase transition around 20 GPa. When the pressure was released, rocksalt type AlN would partially recover to the wurtzite phase below 1.3 GPa, thus two-phase coexistence [77]. Ibáñez et al. studied the high-pressure optical absorption on InN epilayers with the scope of free-electron concentrations to investigate the effect of the optical band gap of wurtzite InN, brought by the free carriers on the pressure coefficient [78].

4 Electrical modulations

As discussed earlier, the development of micro-nano technologies has improved the electrical measurement of 2D materials under compression. For 2D materials, electronic band structure can be modulated by increasing the pressure, thus tuning the electrical transport. Increasing the applied pressure always results in a large increase in conductivity by reducing the cell volume and enhancing the electron orbital level and thereby promoting orbital overlap. Expectedly, the conductivity varies by several orders of magnitude upon compression, which is considered a powerful tool for actuating many electronic transformations under high pressure. Meanwhile, pressure is considered as an efficient strategy to achieve superconducting properties, which can significantly reduce energy consumption.

4.1 Graphene

As shown in Fig. 4(a), after the high-quality trilayer graphene transferred on the diamond surface, Ti/Au film electrodes were then prepared by the use of photo-lithography and electron beam deposition techniques, which were in contact with the sample. Thin platinum foil electrodes were connected to the Ti/Au electrodes at the edge of insulating chamber to maintain current flow under compression. To ensure the insulation between the probing electrodes and the metallic gasket, the indentation area of gasket was covered with a mixture of cubic boron nitride and epoxy [43].

The resistance of two fit lines with different slopes was investigated at ambient temperature with increasing pressure, as was shown in Fig. 4(b). Below 30.1 GPa, the resistance of Bernal-stacked trilayer graphene changed smoothly with the increasing pressure. A break in the trend could be observed at about 33 GPa,

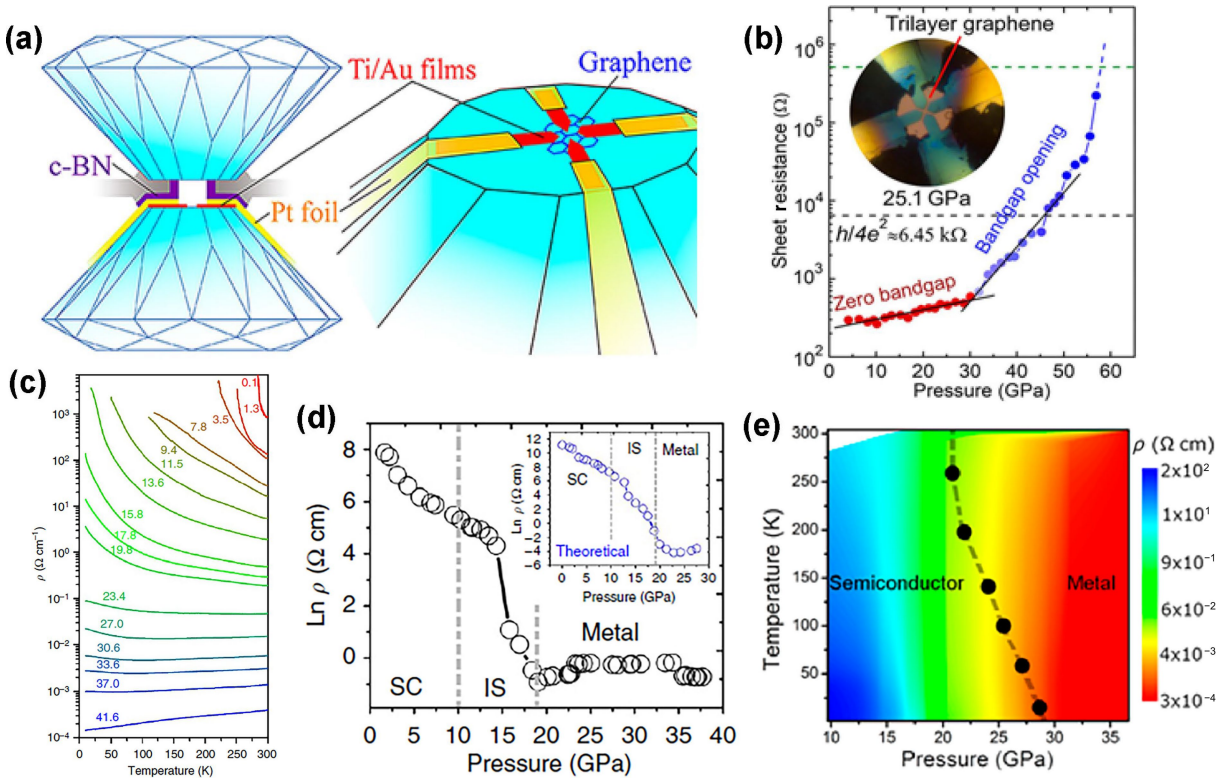

Figure 4 (a) Illustration of a cross-sectional view of the designed microcircuit and a perspective view of the designed microwiring setup. (b) Resistance-pressure curves of trilayer graphene measured at room temperature. (a) and (b) are reproduced with permission from Ref. [42], © The Owner Societies 2016. (c) The side view of 2Hc structure in MoS_2, $MoSe_2$ and $MoTe_2$. Reproduced with permission from Ref. [62], © The Author(s) 2015. (d) Pressure-dependent electrical resistivity of MoS_2. Reproduced with permission from Ref. [36], © American Chemical Society 2014. (e) Temperature-pressure contour plot of resistivity showing the transition region from the semiconductor to metallic region that is derived from experimental electrical conductivity measurements in a DAC. Reproduced with permission from Ref. [87], © American Chemical Society 2015.

following a sudden increase in the resistance at higher pressure. The resistance increased rapidly by more than three orders of magnitudes upon further compression to 59.0 GPa, which was consistent with strong indication of band gap opening. To verify the band gap opening, they also investigated the band gap variation with temperature. The resistance displayed a weak temperature dependence, indicating the semimetallic character at low pressure (below 30.1 GPa). However, the resistance revealed strong temperature-dependent and increased prominently with decreasing temperature above 33.9 GPa, exhibiting a typical semiconducting behavior. Similarly, Amsler et al. and Wang et al. conducted a series of experiments and demonstrated the phase transition from graphene or graphite to the self-defined Z-carbon, which was formed by pure sp^3 bonds under high pressure. These authors also predicted via calculations that Z-carbon revealed a band gap wider than that of semimetallic graphene [79, 80].

4.2 2D perovskites

The crystal and band structure modulations are accompanied by changes in the conductivity of 2D perovskite materials. It is not surprising that change in electrical conductivity reaches orders of magnitude increase due to the narrowing band gap upon compression and pressure has been utilized as an effective method to tune the electrical properties of 3D perovskites [81–85]. For the 2D perovskites, Jaffe studied 2D copper(II)-chloride perovskite and investigated the resistivity through the two-probe DC resistivity measurements conducted within the DAC. The conductivity increased by 5 orders of magnitude under the increasing pressures between 7 to 50 GPa, with a maximum measured conductivity of 2.9×10^{-4} S·cm^{-1} at 51.4 GPa. The conductivity data indicated that (EDBE)[$CuCl_4$] (EDBE = 2,2′-(ethylenedioxy) bis(ethylammonium)) had not achieved a metallic state and it behaved as a semiconductor at increasing pressures, which was consistent with the narrowing band gap [86]. Considering the real photovoltaic applications, electrical response to visible light appears to be particularly important. Besides, upon recompression, some pressure-treated perovskites presented a significantly higher photocurrent than the original sample, owing to the improved structural stability through pressure [85]. Although the photocurrent response under pressure regulation is rarely studied, we can expect a promising result for the photocurrent under compression due to the synergistic contributions of promoting stability and conductivity.

4.3 2D TMDs

Layered TMDs have been identified as exciting material systems with tuning band gap and unique electronic properties under manipulated pressure. As shown in Fig. 4(c), Zhao et al. systematically investigated the conductivity of $MoSe_2$ with increasing pressure up to 60 GPa. At low pressures below 23.4 GPa, the temperature-resistivity curves exhibited negative slopes throughout all temperatures, indicating the semiconductor behavior. Then at the higher pressure from 27.0 to 37.0 GPa, the high-temperature region presented positive slopes, while the low-temperature region was opposite. At above 41.0 GPa, positive slopes could be observed in all temperatures, revealing the metallization of $MoSe_2$. It exhibited highly tunable electronic transport properties under compression, depending on the band

gap narrowing and the following metallization [62]. A similar phenomenon was also observed in MoS_2 [37, 56]. As shown in Fig. 4(d), Nayak et al. conducted the *in situ* resistance measurements at room temperature by the use of standard four-point metallic contacts and demonstrated an electronic transition from a semiconducting to a metallic state at about 19 GPa, caused by a structural lattice distortion [37]. The metallization resulted from the overlap of the valance and conduction bands because interlayer spacing was reduced under high pressure thus enhancing the S-S interactions. It displayed a gradual decrease in resistivity with pressure up to 10 GPa, which could be considered to be caused by a pressure-activated carrier transport. A drastic decrease of resistivity with about three orders of magnitude was observed between the pressure of 10–19 GPa, which was identified as a vanishing band gap due to an S-M electronic transition through theoretical ab initio band structure calculations. Chi et al. reported that MoS_2 metallicized after the phase transition from 2Hc to 2Ha at approximately 40 GPa and proved that the transition was reversible after the pressure was quenched [56].

The same semiconductor-to-metallic transition was observed in the 2D Tungsten disulfide (WS_2) under high pressure. As shown in Fig. 4(e), Nayak et al. reported the transition at around 22 GPa at 280 K, which resulted from increased sulfur-sulfur interactions due to the decreased interlayer spacing under compression. The metallization of WS_2 could be considered a 2D-to-3D phase transition, which is different from those observed in other TMD compounds. The transition led to a substantial regulation of the charge carrier characteristics covering a 2-order decrease in mobility, a 4-order increase in carrier concentration, of course, a 6-order decrease in resistivity [87].

For the homologous compound WTe_2 and $MoTe_2$, superconductivity even could be observed under high pressure. Pan et al. boosted the electronic properties by using high pressure and demonstrated the pressure-induced superconductivity, which was motivated by sensitivity of Te-5p and W-5d orbitals to variations caused by external pressure and strain. The superconductivity appeared at a pressure of 2.5 GPa, rapidly reaching a maximum critical temperature (7 K) at about 16.8 GPa, then by a monotonic decrease in *Tc* with the increasing pressure, thereby indicating the typical dome-shaped superconducting phase [88]. Kang et al. also reported the emergence of superconductivity in pressurized tungsten ditelluride with the suppression of large magnetoresistance, without structural phase transition [89]. Besides, Xia et al. demonstrated a phase transition in semimetallic WTe_2 from an orthorhombic Td phase to a monoclinic T′ phase at 8 GPa, where the Weyl states vanished in the new phase because of the presence of inversion symmetry [90]. For the cognate $MoTe_2$, Qi et al. found that bulk $MoTe_2$ exhibited superconductivity with a transition temperature of 0.10 K. By applying high pressure, the transition temperature was dramatically enhanced up to a maximum value of 8.2 K at 11.7 GPa, which may provide insights into the interaction between superconductivity and two-dimensional topological physics [91]. For the CdI_2, an insulator at ambient conditions, Yan et al. demonstrated that the temperature-dependent resistance indicated an insulator-to-semiconductor transition and followed metallic transition at 36 and 62 GPa, with the band gap shrinking gradually and then a sharp drop at 34.5 GPa. It matched with a first-order transition from a hexagonal to monoclinic phase and a second structural phase transition from monoclinic to tetragonal under increasing pressure [92].

4.4 2D heterostructures

We have discussed the modulations of fundamental characteristics of individual 2D graphene and MoS_2 under compression respectively, and we can expect a promising regulation of electrical properties of graphene by applying hydrostatic pressures onto the heterostructured graphene and monolayer 2H-MoS_2 stacked layers, which can help to understand the physics of 2D materials in extreme environments. As shown in Figs. 5(a) and 5(b), Pandey et al. reported the influence of hydrostatic pressure on the vertically stacked heterostructure formed by monolayer graphene and monolayer 2H-MoS_2, which could lead to p-type doping of graphene through the charge transfer between the heterostructure [93]. A linear shift in Dirac point of graphene was observed with respect to Fermi level through electronic structure calculations under hydrostatic pressure. This shift was quantified by use of doping concentration as a function of hydrostatic pressure. This eventually caused the upward-moving Dirac point, resulting in the enhanced doping. The Bader charge transfer revealed that the charge accumulation on the MoS_2 layer increased as the hydrostatic pressure increased (Fig. 5(d)), with the depleted charge from graphene layer, which indicated an increase in the rate of charge transfer from graphene to MoS_2 with increasing pressure. This is not unexpected, due to the stronger interaction between the two materials with decreasing interlayer spacing, which suggested that electrons flowed from the Dirac point of graphene toward monolayer MoS_2. It was confirmed by the Raman spectra, in which the G band of graphene was strongly dependent on the increasing pressure and shifted at a much higher rate than that of the freestanding graphene. It was shown that applied pressure strongly promoted charge transfer doping between graphene and the monolayer MoS_2, making pressure a prominent method to modulate the doping concentration of graphene or potentially other vdW 2D materials, which was also anticipated by the theoretical insights [93].

The massless Dirac fermions arising from Dirac points are typically considered responsible for remarkable transport properties. Carrier doping often helps tune the Fermi level through the Dirac point to probe the surface-state carriers. In this case, pressure-induced band broadening may shift the Fermi level upward by enhancing the carrier density and help tune the Fermi level toward the Dirac points, possibly producing exotic transport signatures [94, 95].

Liu et al. systematically studied the pressure-modified electronic and lattice structures of $PtTe_2$ via *in situ* transport measurements and X-ray diffraction and distinguished the effect of bulk states from the tilted Dirac nodes on the transport properties [96]. Bykov et al. conducted the high-pressure synthesis of BeN_4, a Dirac material, which represented a qualitatively new class of 2D materials consisting of a metal atom, polymeric nitrogen chains, and host anisotropic Dirac fermions [97].

α-$(BEDT\text{-}TTF)_2I_3$, a 2D organic material, where BEDT-TTF stands for bis(ethylenedithio)-tetrathiafulvalene, has been proven to be an ideal 2D chiral-electron system possessing experimentally accessible charge-neutral Dirac points under hydrostatic pressure. Yakushi et al. demonstrated the charge distributions in the donor layer for the paramagnetic semimetal-like and nonmagnetic insulating phases of the a-$(BEDT\text{-}TTF)_2I_3$ single crystal under pressures of up to 3.6 GPa using Raman spectroscopy [98]. Konoike et al. measured the specific heat of the multilayered material under pressure. The temperature dependence of the specific heat is almost quadratic at a low temperature, suggesting massless Dirac dispersion in this system [99]. Pressure-dependent

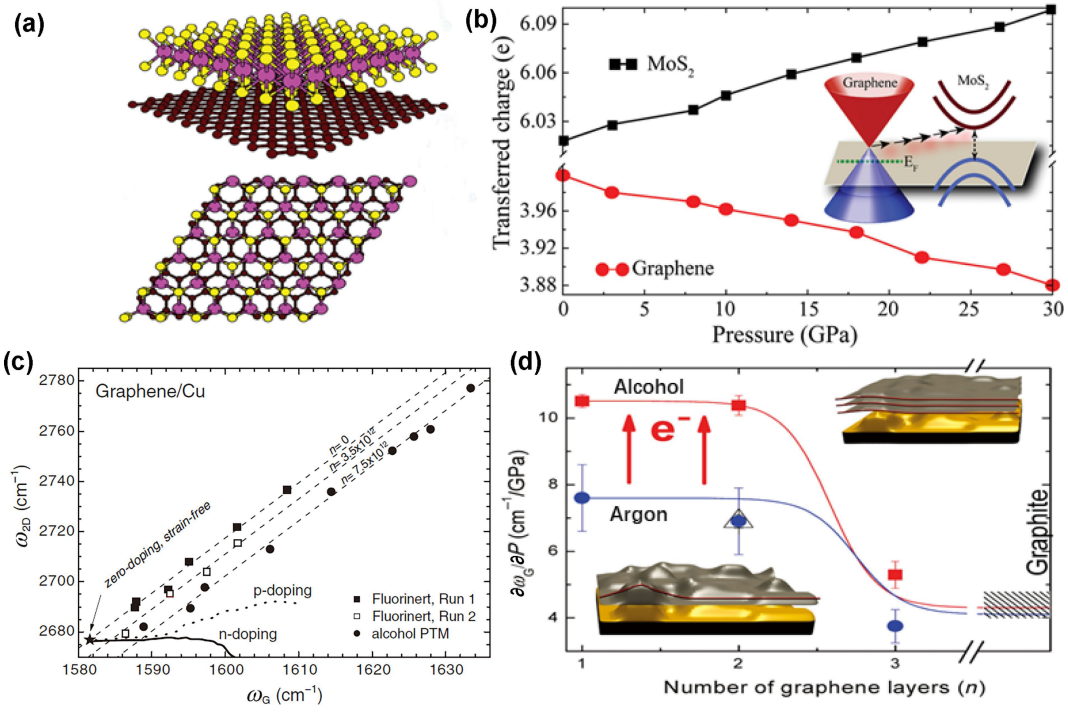

Figure 5 (a, b) Structural properties of graphene/MoS_2 heterostructure and schematic describing the relation between the charge transfer and the shift of the Dirac cone (doping). Reproduced with permission from Ref. [93], © WILEY-VCH Verlag GmbH & Co. KGaA, Weinheim 2016. (c) Correlation between the frequencies, as obtained from the high-pressure Raman spectra, of the G and 2D bands of graphene on Cu substrate. (d) Summary of the G band pressure linear coefficients obtained in alcohol (red squares), argon (blue circles), and nitrogen (green triangle) depending on the number of layers. (c) and (d) are reproduced with permission from Ref. [53], © American Physical Society 2013.

optical investigations of this material have also been performed, and the results demonstrate the tuning charge order and narrow gap of Dirac semimetals [100].

4.5 Influence of a supporting substrate under pressure

As mentioned previously, Machon et al. reported the important role of a supporting substrate for producing biaxial strain conditions under compression and expounded that Raman shifts observed during increasing pressure more likely to be related to the strain induced by the different substrates rather than by the direct pressure [60]. As shown in Fig. 5(c), Filintoglou et al. investigated the charge transfer behavior of graphene on polycrystalline copper under compression with different pressure-transmitting media by the use of Raman spectra. Their analysis revealed that the effect of charge transfer induced by pressure was negligible and it was determined by the compressibility of the substrate and the interaction between the substrate and graphene, and the pressure-transmitting media. This plot was shown by the use of the frequencies of the G and the 2D bands of graphene observed from the high-pressure Raman spectra, in which we could know different pressure transmission media had a great influence on the concentration of charge transfer [53, 101].

Further on, Nicolle et al. performed a series of high-pressure experiments of few-layer graphene samples supported on SiO_2 substrates with alcohol (red squares), argon (blue circles), or nitrogen as pressure-transmitting media. As shown in Fig. 5(d), for samples enfolded by the alcohol, an electron transfer could be observed in monolayer and bilayer graphene, resulting in the doping value of $n \sim 6 \times 10^{13}$ cm^{-2} at the maximum pressure of 7 GPa, which might be caused by formation of silanol groups on the substrate. However, this phenomenon disappeared in trilayer samples and the samples immersed in the pressure-transmitting media of argon or nitrogen [44].

5 Thermal modulations

The thermal conductivity of 2D materials is governed by electrons and phonons. The electronic thermal conductivity (k_e) is related to the electrical conductivity according to the Wiedemann-Franz law (k_e=$L\sigma T$). As discussed above, the electrical properties tuned by high pressure can also cause a difference in k_e. Phonons, defined as the quantum energy of lattice vibration, contribute to the total thermal conductivity, which can be described by a simple kinetic theory:

$$k_l = \frac{1}{3}\sum_i C_v v_i l_i \quad (1)$$

where k_l is the lattice thermal conductivity, C_v is the heat capacity, v_i is the phonon group velocity, and l_i is the phonon mean free path (MFP). When pressure is used to tune the crystal structural parameters, lattice dynamics can be modulated simultaneously. The phonon dispersion can be modified, and the phonon scattering rates can be changed in reciprocal space with the pressure applied to the crystal. Therefore, phonon thermal conductivity can be modulated by changing the phonon group velocity and MFP [102]. Another interesting topic in pressure-tuned thermal properties is interfacial thermal resistance [103]. The interfacial coupling strength is an important factor governing interfacial thermal transport. The vdW interactions within a 2D heterostructure can be easily modified by pressure, thereby tuning interfacial coupling strength.

5.1 *In situ* thermal measurement techniques under pressure

Compared to optical and electrical properties, it is more difficult to test the thermal properties of 2D materials under high pressure,

considering the closed chambers and thermal contact. The use of Raman spectroscopy to measure thermal conductivity is relatively mature in thermal research of 2D materials. The thermal conductivity of the 2D sample can be obtained by testing the temperature difference between the laser center, the edge of the sample, and the light absorption coefficient of the sample [104]. In contrast to the Raman spectroscopic testing method, time-domain thermal reflectance (TDTR) based on femtosecond laser detection technology has unique advantages in terms of measurement accuracy. The TDTR method is used to indirectly obtain the relative change in corresponding temperature by measuring the change in surface reflectance of the metal transducer. It can detect the ultrafast motion of the energy-carrying particles on the interface at the atomic and electronic levels, which can be used to measure the thermal conductivity of 2D thin films and interfacial thermal conductance.

5.2 2D BN

In the section of optical modulation, we discuss the phonon dynamics modulation observed by Raman under pressure. It is also interesting how phonon transport behavior is manipulated under pressure. The transition from h-BN to w-BN has been verified in the pressure-induced experiments and ultrahigh thermal conductivity was predicted in c-BN and w-BN under high pressure [73, 74, 105–109]. As shown in Fig. 6(a), Cuscó et al. showed the relation between phonon frequency and pressure variation through Raman scattering study, in which the interlayer and intralayer E_{2g} Raman-active modes of hexagonal boron nitride were observed under compression. Both the high-frequency mode (E_{2g}^{high}) and the low-frequency mode (E_{2g}^{low}) shifted to higher frequencies with increasing pressure. These frequencies were relevant to the interatomic distances, thus the reduction in lattice parameters leading to their increase with pressure. With the crystal further compressing, it became more difficult to compress, which resulted in a sublinear variation of the lattice parameter with increasing pressure. The higher increasing rate for the E_{2g}^{low} mode can be attributed to the larger compressibility along the *c* direction for 2D h-BN and the strong anisotropy of this material [110]. For the previously reported graphite, an increase of the line intensity of the E_{2g}^{low} mode might be contributed from the interband transition resonances caused by the increasing pressure, which was different from the BN crystal with wide band gap [111].

5.3 2D TMDs

The study of phonon dynamics in TMDs under high pressure had a certain working foundation and the phonon hardening effects had been observed in the interlayer A_{1g} mode and intralayer E_{2g} mode [62, 87]. As shown in Fig. 6(d), Ni et al. revealed the energy relaxation due to the dramatically reduced acoustic phonon scattering with increasing pressure. It was demonstrated by Raman spectroscopy and density functional theory calculations that hydrostatic pressure leads to the increase in the vdW interaction, thus elevating the phonon energies of breathing and shear modes, which provided possible intermediate phonon scattering path between high-frequency optical phonon and acoustic phonon [112]. However, due to the limitation of the test accuracy for thermal conductivity, it is difficult to accurately measure the thermal conductivity changed by the pressure change with Raman spectroscopy.

Meng et al. studied strain-tuned cross-plane thermal conductivity ($k_{\perp}$) in bulk MoS_2 through picosecond transient thermoreflectance (Figs. 6(b) and 6(c)). Cross-plane thermal conductivity increased from 3.5 to 25 $W \cdot m^{-1} \cdot K^{-1}$ with over ~ 9% cross-plane compression created by hydrostatic pressure (19 GPa) in the DAC. Electronic thermal conductivity was obtained via the Wiedemann-Franz law and it could be negligible compared with the total thermal conductivity, which is attributed to the small electron density of states near the Fermi level. Therefore, the substantial increase of thermal conductivity should be caused by the substantially strengthened interlayer force and heavily

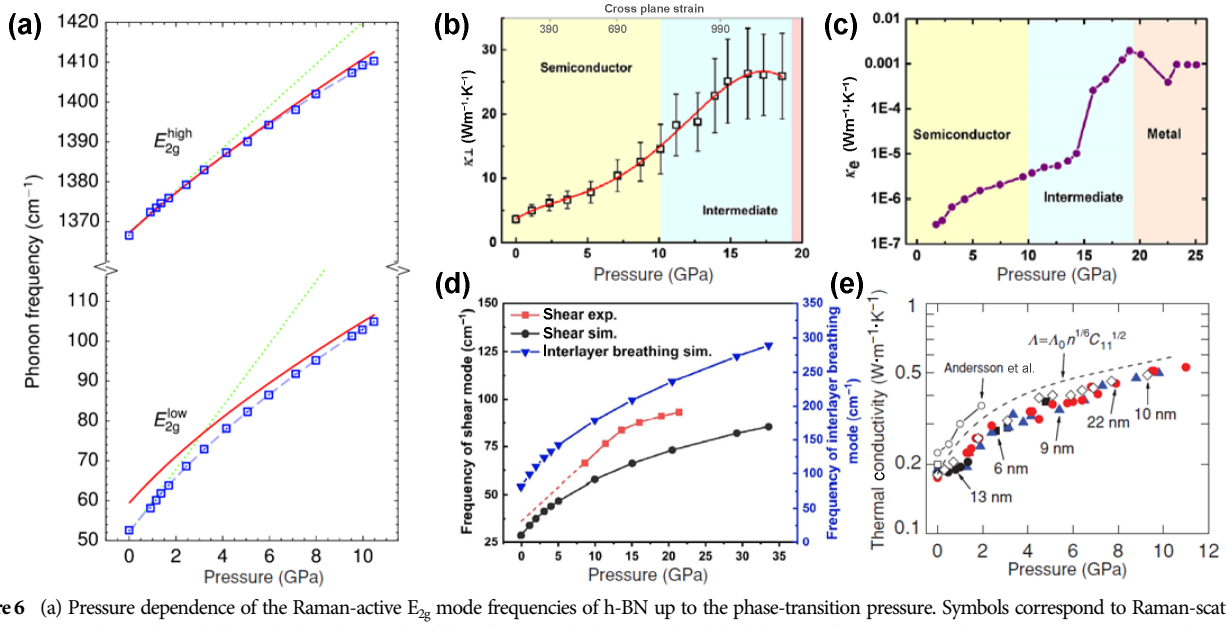

Figure 6 (a) Pressure dependence of the Raman-active E_{2g} mode frequencies of h-BN up to the phase-transition pressure. Symbols correspond to Raman-scattering measurements whereas the solid line displays the results of the *ab initio* calculations. The dashed line is a fit to a Murnaghan-type expression. Reproduced with permission from Ref. [108], © American Physical Society 2011. (b) Extracted total cross-plane thermal conductivity of MoS_2 as a function of pressure. (c) Electronic thermal conductivity of MoS_2 against pressure, determined from measured electrical conductivity via the Wiedemann-Franz law. Reproduced with permission from Ref. [112], © American Physical Society 2021. (d) Frequencies of the shear mode obtained from experiment and simulation and the frequency of interlayer breathing mode from simulation as a function of pressure. Reproduced with permission from Ref. [111], © The American Physical Society 1989. (e) Measurements of the thermal conductivity of PMMA brushes under compression. Reproduced with permission from Ref. [113], © American Physical Society 2019.

modified phonon dispersions along the cross-plane direction, along with the increasing phonon group velocities due to phonon hardening, under compression [113].

5.4 Flexible materials

As shown in Fig. 6(e), Hsieh et al. measured the thermal conductivity of poly(methyl methacrylate) (PMMA) with the increasing pressure through the combination of TDTR and DAC techniques [114]. Compared to the prior experimental work on the thermal conductivity of polymers under limited pressure (up to 2 GPa), this technique could easily generate the high pressures needed to significantly alter the elastic constants of a polymer, and further investigate the modulated thermal conductivity [115–117]. PMMA brushes were independent of the thickness when h>6 nm and increased monotonically with increasing pressure, which was resulted from reduction of the density of localized vibrations at high pressures and further suppressing contributions to thermal transport from localized modes and anharmonic effects. These combined techniques were further used to study the thermal conductivity of layered muscovite crystal [118]. It was found that the thermal conductivity varied from the anomalously low value of 0.46 $W{\cdot}m^{-1}{\cdot}K^{-1}$ at ambient pressure to a value more typical of oxides crystals with large unit cells, 6.6 $W{\cdot}m^{-1}{\cdot}K^{-1}$, at P = 24 GPa. Most of the pressure-induced enhancement of thermal conductivity could be accounted for by the pressure dependence of the cross-plane sound velocities, which suggested that acoustic phonons were the dominant heat carriers in the cross-plane direction in muscovite with large group velocities [118].

Therefore, the thermal conductivity of 2D materials always increases with the increasing pressure, owing to the reduction of electron-phonon scattering resulted from highly localized electronics, achieving higher symmetry suppressing phonon-phonon scattering, increased phonon group velocity, enlarged the band gap of optical phonons and acoustic phonons [106, 119, 120]. The pressure provides a new strategy for achieving the materials with ultrahigh thermal conductivity, which can be used for heat management.

5.5 Anomalous pressure dependence of thermal conductivity

However, as the newly discovered materials with high thermal conductivity, boron arsenide was observed an anomalous pressure dependence of the thermal conductivity [121–123], and Li et al. demonstrated that the general rule of monotonic pressure dependence failed when the lowest-order interactions no longer dominate in energy transport [124–126]. More materials were predicted in the calculations to have anomalous thermal conductivities with the increasing pressure, which depended on the separation of acoustic-acoustic or acoustic-optical branch phonons to be dominant. At present, there is a lack of more experimental evidence and systematic theoretical cognition.

6 Magnetic modulations

In pressure regulation research, the presence of pressure chambers may limit the development of magnetic property modulations. At present, there are two ways to overcome this limitation and achieve magnetic modulation under pressure. One is by probing the magnetic states using tunneling and scanning magnetic circular dichroism microscopy measurements under applied pressure, and the other is by utilizing NV centers in diamond to develop monitoring techniques.

6.1 2D CrI_3

As shown in Figs. 7(a) and 7(b), Song et al. demonstrated pressure modulations of magnetic order in the 2D magnet CrI_3 through the first route [127, 128]. It is found that interlayer magnetic coupling could be more than doubled by hydrostatic pressure. In bilayer CrI_3, pressure induced a transition from layered antiferromagnetic to ferromagnetic phase. In trilayer CrI_3, pressure further created coexisting domains of three phases, one ferromagnetic and two antiferromagnetic. Variation in magnetic order was suggested by changes in the stacking arrangement, which could provide ample opportunities for design magnetic phases and functionalities.

Similarly, Li et al. also investigated interlayer magnetism in atomically thin CrI_3 under compression (Fig. 7(c)) [129]. They modified the stacking order in the 2D CrI_3 under applied hydrostatic pressure about 2 GPa and observed an irreversible interlayer antiferromagnetic-to-ferromagnetic transition in atomically thin CrI_3 by magnetic circular dichroism and electron tunneling measurements, which was accompanied by the change of monoclinic-to-rhombohedral stacking order. It is revealed that the interlayer ferromagnetic ground state was established in bulk CrI_3 rather than in native exfoliated thin films.

6.2 Nitrogen-vacancy centers in diamond

In the DAC, Hsieh et al., Lesik et al., and Yip et al. developed monitoring techniques based on nitrogen-vacancy (NV) centers in diamond. The NV centers can act as sensors because their energy levels and the associated spectra are sensitive to strain and magnetic fields [130–132]. Hsieh et al. quantified all normal and shear stress components and demonstrated vector magnetic field imaging, enabling measurement of the pressure-driven phase transition in iron and the complex pressure-temperature phase diagram of gadolinium. A complementary NV-sensing modality using noise spectroscopy enabled the characterization of phase transitions even in the absence of static magnetic signatures. Lesik et al. illustrate the method using two sets of measurements realized at room temperature and low temperature, respectively: the pressure evolution of the magnetization of an iron bead up to 30 gigapascals showing the iron ferromagnetic collapse and the detection of the superconducting transition of magnesium dibromide at 7 gigapascals. By using a single crystal of $BaFe_2(As_{0.59}P_{0.41})_2$ as a benchmark, Yip et al. extracted the superconducting transition temperature, the local magnetic field profile in the Meissner state, and the critical fields. This method offered a distinct tool for probing and understanding a range of quantum many-body systems. Ishizuka et al. investigated the possibility of magnetic phase transition due to a change in the orbital ordering from antiferrodistortive to ferrodistortive under high pressure, in 2D K_2CuF_4 [133].

7 Other modulations

7.1 Material synthesis

In addition to the above-mentioned modulated properties, pressure can be used as a route to produce new materials via phase transitions and chemical reactions, which are triggered by pressure. As shown in Fig. 8(a), Martins et al. obtained the formation of diamondene, a stable and atomically thick two-dimensional diamond material, by double-layer graphene under high-pressure conditions using water as the pressure transmission medium. The results were explained in terms of a breakdown in the Kohn anomaly associated with the finite size of remaining sp^2

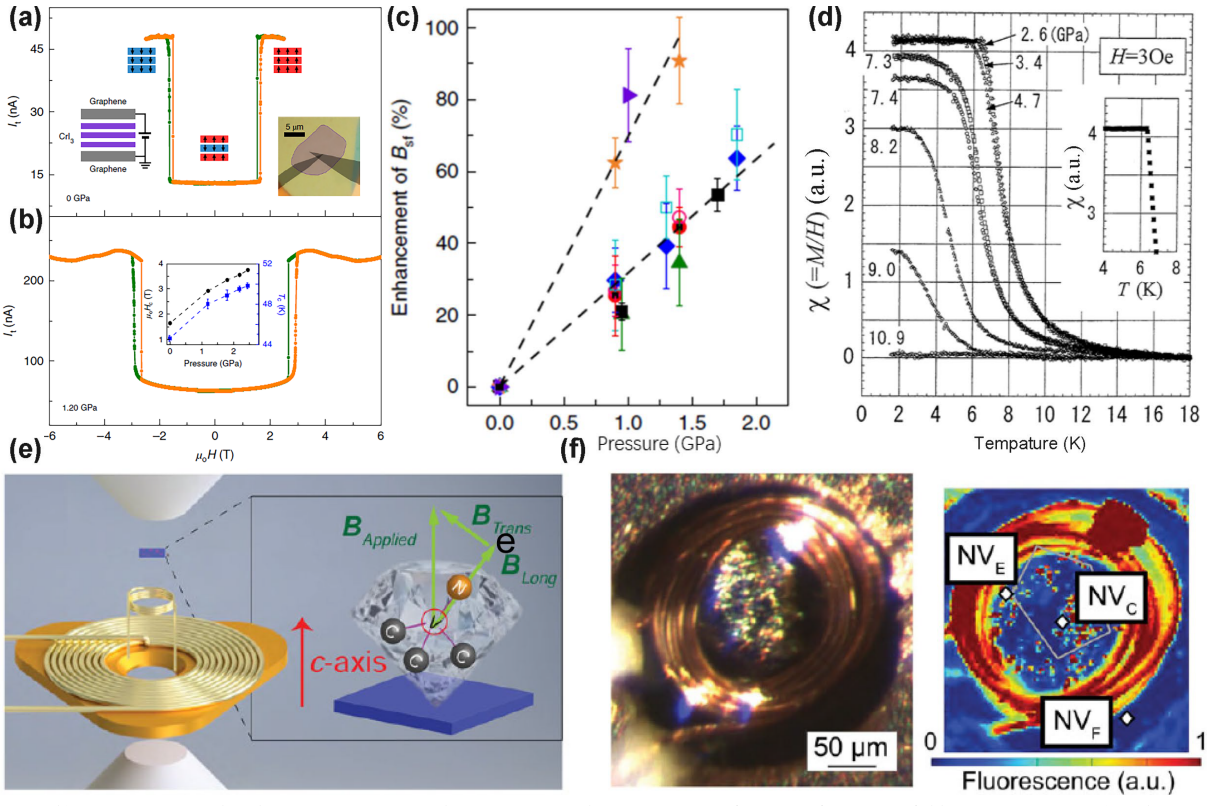

Figure 7 (a, b) New pressure-induced magnetic states in trilayer CrI_3. Tunneling current as a function of magnetic field at zero pressure (a) and 1.2 GPa (b). Reproduced with permission from Ref. [127], © The Author(s), under exclusive licence to Springer Nature Limited 2019. (c) Enhancement of the spin-flip transition field as a function of pressure P from six different devices. Reproduced with permission from Ref. [129], © The Author(s), under exclusive licence to Springer Nature Limited 2019. (d) Temperature dependence of the susceptibility of K_2CuF_4 obtained at various pressures [130]. Reproduced with permission from Ref. [130], © The Author(s) 2019. (e) An exploded view of the pressure cell design. (f) (Left) Photograph of the microcoil with sample on top of the anvil. (Right) Fluorescence image from the confocal scan showing the microcoil and nitrogen-vacancy (NV) centers. (e) and (f) are reproduced with permission from Ref. [132], © The Author(s) 2019.

sites inside the rehybridized 2D matrix, which was confirmed by *ab initio* calculations and molecular dynamics (MD) simulations. Control experiment was performed in single-layer graphene using water as PTM, and also in double-layer graphene using mineral oil as PTM, which indicated that the pressure-induced formation of diamondene was drastically favored by the stacking of two or more layers of graphene surrounded by specific chemical groups such as hydroxyl groups and hydrogens [134, 135]. Similar bonding changes was also achieved by Mao et al. in compressed superhard graphite, as is shown in Fig. 8(c). They considered there was not a complete conversion to a hexagonal diamond, due to not all π-bonds converted into σ-bonds [136]. Similarly, the synthesis w-BN and c-BN were predicted and achieved in the experiments under high pressure [73, 74]. Besides, Yu et al. investigated the 2D $Cr_2Ge_2Te_6$ and revealed the pressure-induced structural phase transition and a special amorphization phase in a DAC [137]. Therefore, pressure provided a convenient route to obtain new materials through phase transitions.

7.2 Thermoelectric materials

Thermoelectric materials have demonstrated great potential in enabling the conversion between thermal and electrical energy, which is especially useful in the face of the current global energy crisis. However, non-ideal thermoelectric performance, as indicated by the figure of merit (ZT), limits the application of thermoelectric materials. Pressure can tune the crystal and band structures, leading to electronic behavior and phonon dispersion modulations. It can also decouple the electrical properties and thermal conductivity, which is considered an effective strategy for ZT enhancement. As mentioned before, the electronic structure controls conductivity, and pressure-driven modulations result in the positive pressure dependence of conductivity. Band structure modulation also contributes to the Seebeck coefficient resulting from the carrier concentration and mobility. Meanwhile, tunable thermal conductivity is predictable under pressure, which can provide a promising method for enhancing thermoelectric performance.

As shown in Fig. 8(d), Chen et al. studied the effects of pressure on ZT in Cr-doped PbSe, which has a maximum ZT of less than 1.0 at a temperature of about 700 K under ambient condition. By applying external pressure using a DAC, a ZT value of about 1.7 could be obtained at room temperature. Through experiments and density functional theory calculations, a pressure-induced topological phase transition was confirmed to enable this enhancement. These findings pointed to the possibility of using compression to increase not just ZT in existing thermoelectric materials, but also the possibility of realizing topological crystalline insulators [138]. Taking advantage of these technical combinations, they also studied the pressure-induced enhancement of thermoelectric performance in PdS and $CuInTe_2$, as well as the half-Heusler compounds [139–142].

8 Conclusion and outlook

2D materials have attracted widespread research interest owing to the abundance of materials with diverse and tunable electrical, optical, and thermal properties, which are closely related to the crystal structures and related energy bands. As illustrated in this

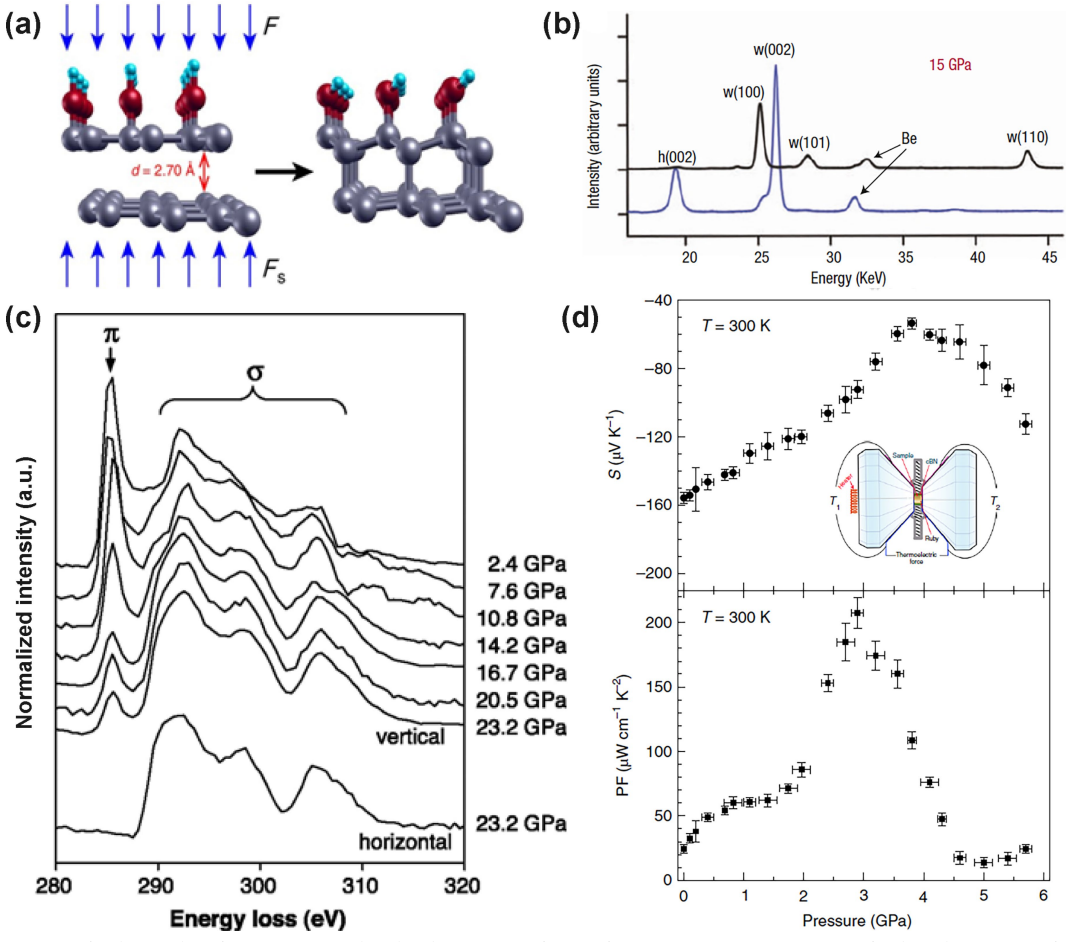

Figure 8 (a) Geometries for diamondene formation. Reproduced with permission from Ref. [121], © American Association for the Advancement of Science 2018. (b) X-ray diffraction patterns of h-BN under 15 GPa. Reproduced with permission from Ref. [73], © Nature Publishing Group 2004. (c) High-pressure IXS spectra for graphite in horizontal and vertical directions plotted as normalized scattered intensity versus energy loss. Reproduced with permission from Ref. [136], © American Association for the Advancement of Science 2003. (d) The Seebeck coefficient and power factor of $Pb_{0.99}Cr_{0.01}Se$ at high pressures. Reproduced with permission from Ref. [138], © The Author(s), under exclusive licence to Springer Nature Limited 2019.

review, pressure modulation is a powerful and extensive tool for simultaneously tuning the crystal and band structures of 2D materials which can modulate their electrical, optical, and thermal properties due to the weak interactions between layers of 2D materials.

With such a powerful tool, further advances can be expected. For example, different surface atom arrangements and electronic structure distributions, which can be precisely tuned by pressure, are important for catalytic efficiency. Due to band structure modulation under pressure, some materials have revealed changes from insulators to metals and even superconductive materials; this phenomenon can provide effective ways to acquire superconductivity. Localized heat in electronic and photonic devices drastically limits the use and development of higher integrated chips, and high thermal conductivity materials are desirable for thermal dissipation. As predicted by previous calculations, high pressure generally enhances phonon group velocity, decreases the electron-phonon scattering, and enlarges the band gap between the optical branches and phonon branches. They may all contribute to higher thermal conductivity, and pressure can provide a more efficient way to modulate thermal conductivity, which can be used in the heat dissipation of electronic devices. Moreover, materials whose thermal conductivity has an anomalous dependence on pressure have been studied. Based on the atomistic theory, this phenomenon is attributed to competitive heat conduction channels from interactive high-order anharmonicity physics inherent to the unique phonon band structure. Furthermore, the atomistic theory enables a novel pathway for the design of thermal insulation materials with thermal conductivities that have a negative dependence on pressure. Notably, some materials have been proven to exhibit pressure-induced thermoelectric performance enhancement owing to the decoupled modulation of their electrical properties and thermal conductivity, which is beneficial for energy conversion. In addition, the interface of 2D heterostructures, where phonon dynamics are quite different from those of the body part, can be easily modified under pressure. This will provide opportunities to investigate long-lived questions regarding interfacial thermal resistance. Therefore, pressure can greatly promote studies of 2D materials and expand their properties and applications through effective modulations.

However, there are also challenges associated with high-pressure technology: (1) The physical mechanisms of pressure modulation require a deep understanding of this new research topic. (2) Ensuring the reliability and precision of pressure-dependent properties also require further development of advanced characterization techniques for *in situ* experiments. (3) The samples placed in the high-pressure apparatus are normally very small, which limits the *in situ* measurement and subsequent applications. For example, the construction of electrocatalytic

devices is difficult to achieve in a DAC chamber because the anvil size is only hundreds of microns, and the converted gas products are difficult to collect and test in time because of the confined environment in the DAC. ④ The extremely high pressure induced by the DAC device is difficult to realize in general situations, which limits the applications of DAC in catalysis, thermoelectrics and other energy conversions. These challenges call for further exploration from both perspectives of fundamental understanding and applications.

Acknowledgements

The authors acknowledge the micro-fabrication center of National Laboratory of Solid State Microstructures (NLSSM) for technique support. Prof. Jia Zhu acknowledges the support from the XPLORER PRIZE. This work is jointly supported by the National Key Research and Development Program of China (No. 2021YFA140070), the National Natural Science Foundation of China (Nos. 61735008, 51925204, 12022403), Excellent Research Program of Nanjing University (ZYJH005), Carbon Peaking and Carbon Neutrality Science and Technology Innovation Fund of Jiangsu Province (BK20220035).

Declaration of conflicting interests

The authors declare no conflicting interests regarding the content of this article.

References

[1] Cai, Z.; Liu, B.; Zou, X.; Cheng, H. M. Chemical vapor deposition growth and applications of two-dimensional materials and their heterostructures. *Chem. Rev.* **2018**, *118*, 6091–6133.

[2] Pei, S.; Wang, Z.; Xia, J. High pressure studies of 2D materials and heterostructures: A review. *Mater. Design* **2022**, *213*, 110363.

[3] Duan, X. D.; Wang, C.; Pan, A. L.; Yu, R. Q.; Duan, X. F. Two-dimensional transition metal dichalcogenides as atomically thin semiconductors: opportunities and challenges. *Chem. Soc. Rev.* **2015**, *44*, 8859–8876.

[4] Lemme, M.; Akinwande, D.; Huyghebaert, C.; Stampfer, C. 2D materials for future heterogeneous electronics. *Nat. Commun.* **2022**, *13*, 1392.

[5] Safaei, J.; Wang, G. Progress and prospects of two-dimensional materials for membrane-based osmotic power generation. *Nano Res. Energy* **2022**, *1*, e9120008.

[6] Chang, C.; Chen, W.; Chen, Y.; Chen, Y.; Chen, Y.; Ding, F.; Fan, C.; Fan, H. J.; Fan, Z.; Gong, C. et al. Recent progress on two-dimensional materials. *Acta Phys. -Chim. Sin* **2021**, *37*, 2108017.

[7] Duan, X.; Wang, C.; Shaw, J. C.; Cheng, R.; Chen, Y.; Li, H.; Wu, X.; Tang, Y.; Zhang, Q.; Pan, A.; Jiang, J.; Yu, R.; Huang, Y.; Duan, X. Lateral epitaxial growth of two-dimensional layered semiconductor heterojunctions. *Nat. Nanotechnol.* **2014**, *9*, 1024–1030.

[8] Mao, H.-K.; Chen, B.; Chen, J.; Li, K.; Lin, J.-F.; Yang, W.; Zheng, H. Recent advances in high-pressure science and technology. *Matter Radiat. Extrem.* **2016**, *1*, 59–75.

[9] Mao, H. -K.; Chen, X. -J.; Ding, Y.; Li, B.; Wang, L. Solids, liquids, and gases under high pressure. *Rev. Mod. Phys.* **2018**, *90*, 01507.

[10] Zhang, L.; Wang, Y.; Lv, J.; Ma, Y. Materials discovery at high pressures. *Nat. Rev. Mater.* **2017**, *2*, 17005.

[11] Xu, M.; Li, Y.; Ma, Y. Materials by design at high pressures. *Chem. Sci.* **2022**, *13*, 329–344.

[12] Su, H.; Zhang, H.; Wu, W.; Wang, X.; Wang, G.; Zhou, L. Chemically engineered dendrite growth of uniform monolayers MoS_2 for enhanced photoluminescence. *Chin. Opt. Lett.* **2022**, *20*, 011602.

[13] Zeng, M.; Liu, J.; Zhou, L.; Mendes, R. G.; Dong, Y.; Zhang, M. Y.; Cui, Z. H.; Cai, Z.; Zhang, Z.; Zhu, D. et al. Bandgap tuning of two-dimensional materials by sphere diameter engineering. *Nat. Mater.* **2020**, *19*, 528–533.

[14] Bai, Y.; Zhou, L.; Wang, J.; Wu, W.; McGilly, L. J.; Halbertal, D.; Lo, C. F. B.; Liu, F.; Ardelean, J.; Rivera, P. et al. Excitons in strain-induced one-dimensional moire potentials at transition metal dichalcogenide heterojunctions. *Nat. Mater.* **2020**, *19*, 1068–1073.

[15] Fan, W.; Zhu, X.; Ke, F.; Chen, Y.; Dong, K.; Ji, J.; Chen, B.; Tongay, S.; Ager, J. W.; Liu, K. et al. Vibrational spectrum renormalization by enforced coupling across the van der Waals gap between MoS_2 and WS_2 monolayers. *Phys. Rev. B* **2015**, *92*.

[16] Rooney, A. P.; Kozikov, A.; Rudenko, A. N.; Prestat, E.; Hamer, M. J.; Withers, F.; Cao, Y.; Novoselov, K. S.; Katsnelson, M. I.; Gorbachev, R. et al. Observing imperfection in atomic interfaces for van der Waals heterostructures. *Nano Lett.* **2017**, *17*, 5222–5228.

[17] Xia, J.; Yan, J.; Wang, Z.; He, Y.; Gong, Y.; Chen, W.; Sum, T. C.; Liu, Z.; Ajayan, P. M.; Shen, Z. Strong coupling and pressure engineering in WSe_2–$MoSe_2$ heterobilayers. *Nat. Phys.* **2020**, *17*, 92–98.

[18] Chen, M.; Xia, J.; Zhou, J.; Zeng, Q.; Li, K.; Fujisawa, K.; Fu, W.; Zhang, T.; Zhang, J.; Wang, Z. et al. Ordered and atomically perfect fragmentation of layered transition metal dichalcogenides via mechanical instabilities. *ACS Nano* **2017**, *11*, 9191–9199.

[19] Conley, H. J.; Wang, B.; Ziegler, J. I.; Haglund, R. F., Jr.; Pantelides, S. T.; Bolotin, K. I. Bandgap engineering of strained monolayer and bilayer MoS_2. *Nano Lett.* **2013**, *13*, 3626–3630.

[20] Yankowitz, M.; Jung, J.; Laksono, E.; Leconte, N.; Chittari, B. L.; Watanabe, K.; Taniguchi, T.; Adam, S.; Graf, D.; Dean, C. R. Dynamic band-structure tuning of graphene moire superlattices with pressure. *Nature* **2018**, *557*, 404–408.

[21] Hui, Y. Y.; Liu, X.; Jie, W.; Chan, N. Y.; Hao, J.; Hsu, Y.-T.; Li, L.-J.; Guo, W.; Lau, S. P. Exceptional tunability of band energy in a compressively strained trilayer MoS_2 sheet. *ACS Nano* **2013**, *7*, 7126–7131.

[22] Wang, J.; Su, R.; Xing, J.; Bao, D.; Diederichs, C.; Liu, S.; Liew, T. C. H.; Chen, Z.; Xiong, Q. Room temperature coherently coupled exciton-polaritons in two-dimensional organic-inorganic perovskite. *ACS Nano* **2018**, *12*, 8382–8389.

[23] Tsai, H.; Nie, W.; Blancon, J. C.; Stoumpos, C. C.; Asadpour, R.; Harutyunyan, B.; Neukirch, A. J.; Verduzco, R.; Crochet, J. J.; Tretiak, S. et al. High-efficiency two-dimensional Ruddlesden-Popper perovskite solar cells. *Nature* **2016**, *536*, 312–316.

[24] Dou, L.; Wong, A. B.; Yu, Y.; Lai, M.; Kornienko, N.; Eaton, S. W.; Fu, A.; Bischak, C. G.; Ma, J.; Ding, T. et al. Atomically thin two-dimensional organic-inorganic hybrid perovskites. *Science* **2015**, *349*, 1518–1521.

[25] Liu, S.; Sun, S.; Gan, C. K.; del Águila, A. G.; Fang, Y.; Xing, J.; Do, T. T. H.; White, T. J.; Li, H.; Huang, W. et al. Manipulating efficient light emission in two-dimensional perovskite crystals by pressure-induced anisotropic deformation. *Sci. Adv.* **2019**, *5*, eaav9445.

[26] Mao, L.; Stoumpos, C. C.; Kanatzidis, M. G. Two-dimensional hybrid halide perovskites: principles and promises. *J. Am. Chem. Soc.* **2019**, *141*, 1171–1190.

[27] Liu, G.; Kong, L.; Yang, W.; Mao, H.-K. Pressure engineering of photovoltaic perovskites. *Mater. Today* **2019**, *27*, 91–106.

[28] Liu, G.; Gong, J.; Kong, L.; Schaller, R. D.; Hu, Q.; Liu, Z.; Yan, S.; Yang, W.; Stoumpos, C. C.; Kanatzidis, M. G. et al. Isothermal pressure-derived metastable states in 2D hybrid perovskites showing enduring bandgap narrowing. *Proc. Natl. Acad. Sci. USA* **2018**, *115*, 8076–8081.

[29] Kong, L.; Liu, G.; Gong, J.; Hu, Q.; Schaller, R. D.; Dera, P.; Zhang, D.; Liu, Z.; Yang, W.; Zhu, K. et al. Simultaneous band-gap narrowing and carrier-lifetime prolongation of organic-inorganic trihalide perovskites. *Proc. Natl. Acad. Sci. USA* **2016**, *113*,

8910–8915.
[30] Xiao, G.; Cao, Y.; Qi, G.; Wang, L.; Liu, C.; Ma, Z.; Yang, X.; Sui, Y.; Zheng, W.; Zou, B. Pressure effects on structure and optical properties in cesium lead bromide perovskite nanocrystals. *J. Am. Chem. Soc.* **2017**, *139*, 10087–10094.
[31] Zhu, H.; Cai, T.; Que, M.; Song, J.-P.; Rubenstein, B. M.; Wang, Z.; Chen, O. Pressure-induced phase transformation and band-gap engineering of formamidinium lead iodide perovskite nanocrystals. *J. Phys. Chem. Lett.* **2018**, *9*, 4199–4205.
[32] Fang, Y.; Zhang, L.; Wu, L.; Yan, J.; Lin, Y.; Wang, K.; Mao, W. L.; Zou, B. Pressure-induced emission (PIE) and phase transition of a two-dimensional halide double perovskite $(BA)_4AgBiBr_8$ ($BA=CH_3(CH_2)_3NH_3^+$). *Angew Chem., Int. Ed.* **2019**, *58*, 15249–15253.
[33] Chen, Y.; Fu, R.; Wang, L.; Ma, Z.; Xiao, G.; Wang, K.; Zou, B. Emission enhancement and bandgap retention of a two-dimensional mixed cation lead halide perovskite under high pressure. *J. Mater. Chem. A* **2019**, *7*, 6357–6362.
[34] Ren, X.; Yan, X.; Gennep, D. V.; Cheng, H.; Wang, L.; Li, Y.; Zhao, Y.; Wang, S. Bandgap widening by pressure-induced disorder in two-dimensional lead halide perovskite. *Appl. Phys. Lett.* **2020**, *116*.
[35] Kong, L.; Liu, G.; Gong, J.; Mao, L.; Chen, M.; Hu, Q.; Lu, X.; Yang, W.; Kanatzidis, M. G.; Mao, H. K. Highly tunable properties in pressure-treated two-dimensional Dion-Jacobson perovskites. *Proc. Natl. Acad. Sci. USA* **2020**, *117*, 16121–16126.
[36] Nayak, A. P.; Pandey, T.; Voiry, D.; Liu, J.; Moran, S. T.; Sharma, A.; Tan, C.; Chen, C. H.; Li, L. J.; Chhowalla, M. et al. Pressure-dependent optical and vibrational properties of monolayer molybdenum disulfide. *Nano Lett.* **2015**, *15*, 346–353.
[37] Nayak, A. P.; Bhattacharyya, S.; Zhu, J.; Liu, J.; Wu, X.; Pandey, T.; Jin, C.; Singh, A. K.; Akinwande, D.; Lin, J. F. Pressure-induced semiconducting to metallic transition in multilayered molybdenum disulphide. *Nat. Commun.* **2014**, *5*, 3731.
[38] Fu, L.; Wan, Y.; Tang, N.; Ding, Y. -M.; Gao, J.; Yu, J.; Guan, H.; Zhang, K.; Wang, W.; Zhang, C.; Shi J.; Wu, X.; Shi, S.; Ge, W.; Dai, J.; Shen, B. K. Λ crossover transition in the conduction band of monolayer MoS_2 under hydrostatic pressure. *Sci. Adv.* **2017**, *3*, e1700162.
[39] Dou, X.; Ding, K.; Jiang, D.; Sun, B. Tuning and identification of interband transitions in monolayer and bilayer molybdenum disulfide using hydrostatic pressure. *ACS Nano* **2014**, *8*, 7458–7464.
[40] Dou, X.; Ding, K.; Jiang, D.; Fan, X.; Sun, B. Probing spin-orbit coupling and interlayer coupling in atomically thin molybdenum disulfide using hydrostatic pressure. *ACS Nano* **2016**, *10*, 1619–1624.
[41] Rifliková, M.; Martoňák, R.; Tosatti, E. Pressure-induced gap closing and metallization of $MoSe_2$ and $MoTe_2$. *Phys. Rev. B* **2014**, *90*, 035108.
[42] Fan, X.; Singh, D. J.; Jiang, Q.; Zheng, W. T. Pressure evolution of the potential barriers of phase transition of MoS_2, $MoSe_2$ and $MoTe_2$. *Phys. Chem. Chem. Phys.* **2016**, *18*, 12080–12085.
[43] Ke, F.; Chen, Y.; Yin, K.; Yan, J.; Zhang, H.; Liu, Z.; Tse, J. S.; Wu, J.; Mao, H. K.; Chen, B. Large bandgap of pressurized trilayer graphene. *Proc. Natl. Acad. Sci. USA* **2019**, *116*, 9186–9190.
[44] Nicolle, J.; Machon, D.; Poncharal, P.; Pierre-Louis, O.; San-Miguel, A. Pressure-mediated doping in graphene. *Nano Lett.* **2011**, *11*, 3564–3568.
[45] Hu, K.; Yao, M.; Yang, Z.; Xiao, G.; Zhu, L.; Zhang, H.; Liu, R.; Zou, B.; Liu, B. Pressure tuned photoluminescence and band gap in two-dimensional layered g-C_3N_4: the effect of interlayer interactions. *Nanoscale* **2020**, *12*, 12300–12307.
[46] Xiang, Z. J.; Ye, G. J.; Shang, C.; Lei, B.; Wang, N. Z.; Yang, K. S.; Liu, D. Y.; Meng, F. B.; Luo, X. G.; Zou, L. J. et al. Pressure-induced electronic transition in black phosphorus. *Phys. Rev. Lett.* **2015**, *115*, 186403.
[47] Polian, A.; Gauthier, M.; Souza, S. M.; Trichês, D. M.; Cardoso de Lima, J.; Grandi, T. A. Two-dimensional pressure-induced electronic topological transition in Bi_2Te_3. *Phys. Rev. B* **2011**, *83*, 113106.
[48] Du, K. Z.; Tu, Q.; Zhang, X.; Han, Q.; Liu, J.; Zauscher, S.; Mitzi, D. B. Two-dimensional lead(II) halide-based hybrid perovskites templated by acene alkylamines: crystal structures, optical properties, and piezoelectricity. *Inorg. Chem.* **2017**, *56*, 9291–9302.
[49] Jaffe, A.; Lin, Y.; Karunadasa, H. I. Halide perovskites under pressure: accessing new properties through lattice compression. *ACS Energy Lett.* **2017**, *2*, 1549–1555.
[50] Qin, Z.; Dai, S.; Gajjela, C. C.; Wang, C.; Hadjiev, V. G.; Yang, G.; Li, J.; Zhong, X.; Tang, Z.; Yao, Y. et al. Spontaneous formation of 2D/3D heterostructures on the edges of 2D Ruddlesden-Popper hybrid perovskite crystals. *Chem. Mater.* **2020**, *32*, 5009–5015.
[51] Ke, F.; Zhang, L.; Chen, Y.; Yin, K.; Wang, C.; Tzeng, Y. K.; Lin, Y.; Dong, H.; Liu, Z.; Tse, J. S. et al. Synthesis of atomically thin hexagonal diamond with compression. *Nano Lett.* **2020**, *20*, 5916–5921.
[52] Proctor, J. E.; Gregoryanz, E.; Novoselov, K. S.; Lotya, M.; Coleman, J. N.; Halsall, M. P. High-pressure Raman spectroscopy of graphene. *Phys. Rev. B* **2009**, *80*, 073408.
[53] Filintoglou, K.; Papadopoulos, N.; Arvanitidis, J.; Christofilos, D.; Frank, O.; Kalbac, M.; Parthenios, J.; Kalosakas, G.; Galiotis, C.; Papagelis, K. Raman spectroscopy of graphene at high pressure: Effects of the substrate and the pressure transmitting media. *Phys. Rev. B* **2013**, *88*, 045418.
[54] Clark, S. M.; Jeon, K.-J.; Chen, J.-Y.; Yoo, C.-S. Few-layer graphene under high pressure: Raman and X-ray diffraction studies. *Solid State Commun.* **2013**, *154*, 15–18.
[55] Lu, S.; Yao, M.; Yang, X.; Li, Q.; Xiao, J.; Yao, Z.; Jiang, L.; Liu, R.; Liu, B.; Chen, S. et al. High pressure transformation of graphene nanoplates: A Raman study. *Chem. Phys. Lett.* **2013**, *585*, 101–106.
[56] Chi, Z. H.; Zhao, X. M.; Zhang, H.; Goncharov, A. F.; Lobanov, S. S.; Kagayama, T.; Sakata, M.; Chen, X. J. Pressure-induced metallization of molybdenum disulfide. *Phys. Rev. Lett.* **2014**, *113*, 036802.
[57] Livneh, T.; Sterer, E. Resonant Raman scattering at exciton states tuned by pressure and temperature in 2H-MoS_2. *Phys. Rev. B* **2010**, *81*, 195209.
[58] Aksoy, R.; Ma, Y.; Selvi, E.; Chyu, M. C.; Ertas, A.; White, A. X-ray diffraction study of molybdenum disulfide to 38.8 GPa. *J. Phys. Chem. Solids* **2006**, *67*, 1914.
[59] Hromadová, L.; Martoňák, R.; Tosatti, E. Structure change, layer sliding, and metallization in high-pressure MoS_2. *Phys. Rev. B* **2013**, *87*, 144105.
[60] Machon, D.; Bousige, C.; Alencar, R.; Torres-Dias, A.; Balima, F.; Nicolle, J.; de Sousa Pinheiro, G.; Souza Filho, A. G.; San-Miguel, A. Raman scattering studies of graphene under high pressure. *J. Raman Spectrosc.* **2018**, *49*, 121–129.
[61] Zhuang, Y.; Dai, L.; Wu, L.; Li, H.; Hu, H.; Liu, K.; Yang, L.; Pu, C. Pressure-induced permanent metallization with reversible structural transition in molybdenum disulfide. *Appl. Phys. Lett.* **2017**, *110*, 122103.
[62] Zhao, Z.; Zhang, H.; Yuan, H.; Wang, S.; Lin, Y.; Zeng, Q.; Xu, G.; Liu, Z.; Solanki, G. K.; Patel, K. D. et al. Pressure induced metallization with absence of structural transition in layered molybdenum diselenide. *Nat. Commun.* **2015**, *6*, 7312.
[63] Geick, R.; Perry, C. H.; Rupprecht, G. Normal modes in hexagonal boron nitride. *Phys. Rev.* **1966**, *146*, 543–547.
[64] Liu, L.; Feng, Y. P.; Shen, Z. X. Structural and electronic properties of h-BN. *Phys. Rev. B* **2003**, *68*, 104102.
[65] Chang, H.-Y.; Yang, S.; Lee, J.; Tao, L.; Hwang, W.-S.; Jena, D.; Lu, N.; Akinwande, D. High-performance, highly bendable MoS_2 transistors with high-K dielectrics for flexible low-power systems. *ACS Nano* **2013**, *7*, 5446–5452.
[66] Schmidt, H.; Wang, S.; Chu, L.; Toh, M.; Kumar, R.; Zhao, W.;

Neto, A. H.; Martin, J.; Adam, S.; Özyilmaz, B.; Eda, G. Transport properties of monolayer MoS_2 grown by chemical vapor deposition. *Nano Lett.* **2014**, *14*, 1909–1913.

[67] Lee, G.-H.; Cui, X.; Kim, Y. D.; Arefe, G.; Zhang, X.; Lee, C.-H.; Ye, F.; Watanabe, K.; Taniguchi, T.; Kim, P.; Hone, J. Highly stable, dual-gated MoS_2 transistors encapsulated by hexagonal boron nitride with gate-controllable contact, resistance, and threshold voltage. *ACS Nano* **2015**, *9*, 7019–7026.

[68] Britnell, L.; Gorbachev, R. V.; Geim, A. K.; Ponomarenko, L. A.; Mishchenko, A.; Greenaway, M. T.; Fromhold, T. M.; Novoselov, K. S.; Eaves, L. Resonant tunnelling and negative differential conductance in graphene transistors. *Nat. Commun.* **2013**, *4*, 1794.

[69] Britnell, L.; Gorbachev, R. V.; Jalil, R.; Belle, B. D.; Schedin, F.; Katsnelson, M. I.; Eaves, L.; Morozov, S. V.; Mayorov, A. S.; Peres, N. M. et al. Electron tunneling through ultrathin boron nitride crystalline barriers. *Nano Lett.* **2012**, *12*, 1707–1710.

[70] Xu, Y. N.; Ching, W. Y. Calculation of ground-state and optical properties of boron nitrides in the hexagonal, cubic, and wurtzite structures. *Phys. Rev. B Condens Matter* **1991**, *44*, 7787–7798.

[71] Furthmüller, J.; Hafner, J.; Kresse, G. *Ab initio* calculation of the structural and electronic properties of carbon and boron nitride using ultrasoft pseudopotentials. *Phys. Rev. B Condens. Matter* **1994**, *50*, 15606–15622.

[72] Wentzcovitch, R. M.; Fahy, S.; Cohen, M. L.; Louie, S. G. *Ab initio* study of graphite→diamondlike transitions in BN. *Phys. Rev. B* **1988**, *38*, 6191–6195.

[73] Meng, Y.; Mao, H. K.; Eng, P. J.; Trainor, T. P.; Newville, M.; Hu, M. Y.; Kao, C.; Shu, J.; Hausermann, D.; Hemley, R. J. The formation of sp^3 bonding in compressed BN. *Nat. Mater.* **2004**, *3*, 111–1114.

[74] Segura, A.; Cuscó, R.; Taniguchi, T.; Watanabe, K.; Cassabois, G.; Gil, B.; Artús, L. Nonreversible transition from the hexagonal to wurtzite phase of boron nitride under high pressure: Optical properties of the wurtzite phase. *J. Phys. Chem. C* **2019**, *123*, 20167–20173.

[75] Saha, S.; Muthu, D. V. S.; Golberg, D.; Tang, C.; Zhi, C.; Bando, Y.; Sood, A. K. Comparative high pressure Raman study of boron nitride nanotubes and hexagonal boron nitride. *Chem. Phys. Lett.* **2006**, *421*, 86–90.

[76] Xia, H.; Xia, Q.; Ruoff, A. L. High-pressure structure of gallium nitride: Wurtzite-to-rocksalt phase transition. *Phys. Rev. B Condens Matter* **1993**, *47*, 12925–12928.

[77] Manjón, F. J.; Errandonea, D.; Romero, A. H.; Garro, N.; Serrano, J.; Kuball, M. Lattice dynamics of wurtzite and rocksalt AlN under high pressure: Effect of compression on the crystal anisotropy of wurtzite-type semiconductors. *Phys. Rev. B* **2008**, *77*, 205204.

[78] Ibáñez, J.; Segura, A.; García-Domene, B.; Oliva, R.; Manjón, F. J.; Yamaguchi, T.; Nanishi, Y.; Artús, L. High-pressure optical absorption in InN: Electron density dependence in the wurtzite phase and reevaluation of the indirect band gap of rocksalt InN. *Phys. Rev. B* **2012**, *86*, 035210.

[79] Amsler, M.; Flores-Livas, J. A.; Lehtovaara, L.; Balima, F.; Ghasemi, S. A.; Machon, D.; Pailhès, S.; Willand, A.; Caliste, D.; Botti, S. et al. Crystal structure of cold compressed graphite. *Phys. Rev. Lett.* **2012**, *108*, 065501.

[80] Wang, J. T.; Chen, C.; Kawazoe, Y. Low-temperature phase transformation from graphite to sp^3 orthorhombic carbon. *Phys. Rev. Lett.* **2011**, *106*, 075501.

[81] Szafrański, M.; Katrusiak, A. Mechanism of pressure-induced phase transitions, amorphization, and absorption-edge shift in photovoltaic methylammonium lead iodide. *J. Phys. Chem. Lett.* **2016**, *7*, 3458–3466.

[82] Lee, Y.; Mitzi, D. B.; Barnes, P. W.; Vogt, T. Pressure-induced phase transitions and templating effect in three-dimensional organic-inorganic hybrid perovskites. *Phys. Rev. B* **2003**, *68*, 020103.

[83] Jaffe, A.; Lin, Y.; Mao, W. L.; Karunadasa, H. I. Pressure-induced metallization of the halide perovskite $(CH_3NH_3)PbI_3$. *J. Am. Chem. Soc.* **2017**, *139*, 4330–4333.

[84] Wang, Y.; Lü, X.; Yang, W.; Wen, T.; Yang, L.; Ren, X.; Wang, L.; Lin, Z.; Zhao, Y. Pressure-induced phase transformation, reversible amorphization, and anomalous visible light response in organolead bromide perovskite. *J. Am. Chem. Soc.* **2015**, *137*, 11144–11149.

[85] Lü, X.; Wang, Y.; Stoumpos, C. C.; Hu, Q.; Guo, X.; Chen, H.; Yang, L.; Smith, J. S.; Yang, W.; Zhao, Y.; Xu, H.; Kanatzidis, M. G.; Jia, Q. Enhanced structural stability and photo responsiveness of $CH_3NH_3SnI_3$ perovskite via pressure-induced amorphization and recrystallization. *Adv. Mater.* **2016**, *28*, 8663–8668.

[86] Jaffe, A.; Lin, Y.; Mao, W. L.; Karunadasa, H. I. Pressure-induced conductivity and yellow-to-black piezochromism in a layered Cu-Cl hybrid perovskite. *J. Am. Chem. Soc.* **2015**, *137*, 1673–1678.

[87] Nayak, A. P.; Yuan, Z.; Cao, B.; Liu, J.; Wu, J.; Moran, S. T.; Li, T.; Akinwande, D.; Jin, C.; Lin, J.-F. Pressure-modulated conductivity, carrier density, and mobility of multilayered tungsten disulfide. *ACS Nano* **2015**, *9*, 9117–9123.

[88] Pan, X. C.; Chen, X.; Liu, H.; Feng, Y.; Wei, Z.; Zhou, Y.; Chi, Z.; Pi, L.; Yen, F.; Song, F.; Wan, X.; Yang, Z.; Wang, B.; Wang, G.; Zhang, Y. Pressure-driven dome-shaped superconductivity and electronic structural evolution in tungsten ditelluride. *Nat. Commun.* **2015**, *6*, 7805.

[89] Kang, D.; Zhou, Y.; Yi, W.; Yang, C.; Guo, J.; Shi, Y.; Zhang, S.; Wang, Z.; Zhang, C.; Jiang, S.; Li, A.; Yang, K.; Wu, Q.; Zhang, G.; Sun, L.; Zhao, Z. Superconductivity emerging from a suppressed large magnetoresistant state in tungsten ditelluride. *Nat. Commun.* **2015**, *6*, 7804.

[90] Xia, J.; Li, D. F.; Zhou, J. D.; Yu, P.; Lin, J. H.; Kuo, J. L.; Li, H. B.; Liu, Z.; Yan, J. X.; Shen, Z. X. Pressure-induced phase transition in weyl semimetallic WTe_2. *Small* **2017**, *13*, 1701887.

[91] Qi, Y.; Naumov, P. G.; Ali, M. N.; Rajamathi, C. R.; Schnelle, W.; Barkalov, O.; Hanfland, M.; Wu, S. C.; Shekhar, C.; Sun, Y. et al. Superconductivity in Weyl semimetal candidate $MoTe_2$. *Nat. Commun.* **2016**, *7*, 11038.

[92] Yan, Z.; Yin, K.; Yu, Z.; Li, X.; Li, M.; Yuan, Y.; Li, X.; Yang, K.; Wang, X.; Wang, L. Pressure-induced band-gap closure and metallization in two-dimensional transition metal halide CdI_2. *Appl. Mater. Tod.* **2020**, *18*, 100532.

[93] Pandey, T.; Nayak, A. P.; Liu, J.; Moran, S. T.; Kim, J. S.; Li, L. J.; Lin, J. F.; Akinwande, D.; Singh, A. K. Pressure-induced charge transfer doping of monolayer graphene/MoS_2 heterostructure. *Small* **2016**, *12*, 4063–4069.

[94] Malavi, P.; Kumar, P.; Jakhar, N.; Singh, S.; Karmakar, S. Signature of superconducting onset in presence of large magnetoresistance in type-II dirac semimetal candidate Ir_2In_8S. *New J. Phys.* **2022**, *24*, 102002.

[95] Hirata, M.; Kobayashi, A.; Berthier, C.; Kanoda, K. Interacting chiral electrons at the 2D dirac points: A review. *Rep. Prog. Phys.* **2021**, *84*, 036502.

[96] Liu, F.; Li, J.; Zhang, K.; Peng, S.; Huang, H.; Yan, M.; Li, N.; Zhang, Q.; Guo, S.; Lu, X. et al. Pressure-induced Lifshitz transition in the type II dirac semimetal $PtTe_2$. *Sci. China Phys. Mech.* **2019**, *62*, 1.

[97] Bykov, M.; Fedotenko, T.; Chariton, S.; Laniel, D.; Glazyrin, K.; Hanfland, M.; Smith, J. S.; Prakapenka, V. B.; Mahmood, M. F.; Goncharov, A. F. et al. High-pressure synthesis of dirac materials: layered van der Waals bonded BeN_4 polymorph. *Phys. Rev. Lett.* **2021**, *126*, 175501.

[98] Wojciechowski, R.; Yamamoto, K.; Yakushi, K.; Inokuchi, M.; Kawamoto, A. High-pressure Raman study of the charge ordering in α-$(BEDT\text{-}TTF)_2I_3$. *Phys. Rev. B* **2003**, *67*, 224105.

[99] Konoike, T.; Uchida, K.; Osada, T. Specific heat of the multilayered massless dirac fermion system. *J. Phys. Soc. Jpn.* **2012**, *81*, 043601.

[100] Beyer, R.; Dengl, A.; Peterseim, T.; Wackerow, S.; Ivek, T.; Pronin, A. V.; Schweitzer, D.; Dressel, M. Pressure-dependent optical investigations of α-$(BEDT\text{-}TTF)_2I_3$: Tuning charge order and narrow gap towards a dirac semimetal. *Phys. Rev. B* **2016**, *93*,

195116.
[101] Klotz, S.; Chervin, J. C.; Munsch, P.; Le Marchand, G. Hydrostatic limits of 11 pressure transmitting media. *J. Phys. D:Appl. Phys.* **2009**, *42*, 075413.
[102] Zhou, Y.; Dong, Z.-Y.; Hsieh, W.-P.; Goncharov, A. F.; Chen, X.-J. Thermal conductivity of materials under pressure. *Nat. Rev. Phys.* **2022**, *4*, 319–335.
[103] Chen, J.; Xu, X.; Zhou, J.; Li, B. Interfacial thermal resistance: Past, present, and future. *Rev. Mod. Phys.* **2022**, *94*, 025002.
[104] Yang, F.; Wang, R.; Zhao, W.; Jiang, J.; Wei, X.; Zheng, T.; Yang, Y.; Wang, X.; Lu, J.; Ni, Z. Thermal transport and energy dissipation in two-dimensional Bi_2O_2Se. *Appl. Phys. Lett.* **2019**, *115*, 193103.
[105] Guerra, V.; Wan, C.; McNally, T. Thermal conductivity of 2D nano-structured boron nitride (BN) and its composites with polymers. *Prog. Mater. Sci.* **2019**, *100*, 170–186.
[106] Chakraborty, P.; Xiong, G.; Cao, L.; Wang, Y. Lattice thermal transport in superhard hexagonal diamond and wurtzite boron nitride: A comparative study with cubic diamond and cubic boron nitride. *Carbon* **2018**, *139*, 85–93.
[107] Segura, A.; Cuscó, R.; Taniguchi, T.; Watanabe, K.; Cassabois, G.; Gil, B.; Artús, L. High-pressure softening of the out-of-plane A_{2u}(transverse-optic) mode of hexagonal boron nitride induced by dynamical buckling. *J. Phys. Chem. C* **2019**, *123*, 17491–17497.
[108] Hromadová, L.; Martoňák, R. Pressure-induced structural transitions in BN from *ab initio* metadynamics. *Phys. Rev. B* **2011**, *84*, 224108.
[109] Chen, K.; Song, B.; Ravichandran, N. K.; Zheng, Q.; Chen, X.; Lee, H.; Sun, H.; Li, S.; Udalamatta Gamage, G. A. G.; Tian, F. et al. Ultrahigh thermal conductivity in isotope-enriched cubic boron nitride. *Science* **2020**, *367*, 555–559.
[110] Cuscó, R.; Pellicer-Porres, J.; Edgar, J. H.; Li, J.; Segura, A.; Artús, L. Pressure dependence of the interlayer and intralayer E_{2g} Raman-active modes of hexagonal BN up to the wurtzite phase transition. *Phys. Rev. B* **2020**, *102*, 075206.
[111] Hanfland, M.; Beister, H.; Syassen, K. Graphite under pressure: Equation of state and first-order Raman modes. *Phys. Rev. B Condens. Matter* **1989**, *39*, 12598–12603.
[112] Ni, K.; Du, J.; Yang, J.; Xu, S.; Cong, X.; Shu, N.; Zhang, K.; Wang, A.; Wang, F.; Ge, L. et al. Stronger interlayer interactions contribute to faster hot carrier cooling of bilayer graphene under pressure. *Phys. Rev. Lett.* **2021**, *126*, 027402.
[113] Meng, X.; Pandey, T.; Jeong, J.; Fu, S.; Yang, J.; Chen, K.; Singh, A.; He, F.; Xu, X.; Zhou, J. et al. Thermal conductivity enhancement in MoS_2 under extreme strain. *Phys. Rev. Lett.* **2019**, *122*, 155901.
[114] Hsieh, W.-P.; Losego, M. D.; Braun, P. V.; Shenogin, S.; Keblinski, P.; Cahill, D. G. Testing the minimum thermal conductivity model for amorphous polymers using high pressure. *Phys. Rev. B* **2011**, *83*, 174205.
[115] Abramson, E. H.; Brown, J. M.; Slutsky, L. J. The thermal diffusivity of water at high pressures and temperatures. *J. Chem. Phys.* **2001**, *115*, 10461–10463.
[116] Frost, R. S.; Chen, R. Y. S.; Barker, R. E. Pressure dependence of thermal conductivity in polyethylene. *J. Appl. Phys.* **1975**, *46*, 4506–4509.
[117] Beck, P.; Goncharov, A. F.; Struzhkin, V. V.; Militzer, B.; Mao, H.-K.; Hemley, R. J. Measurement of thermal diffusivity at high pressure using a transient heating technique. *Appl. Phys. Lett.* **2007**, *91*, 181914.
[118] Hsieh, W.-P.; Chen, B.; Li, J.; Keblinski, P.; Cahill, D. G. Pressure tuning of the thermal conductivity of the layered muscovite crystal. *Phys. Rev. B* **2009**, *80*, 180302.
[119] Xiao, G.; Geng, T.; Zou, B. Emerging functional materials under high pressure toward enhanced properties. *ACS Mater. Lett.* **2020**, *2*, 1233–1239.
[120] Miao, M.; Sun, Y.; Zurek, E.; Lin, H. Chemistry under high pressure. *Nat. Rev. Chem.* **2020**, *4*, 508–527.
[121] Li, S.; Zheng, Q.; Lv, Y.; Liu, X.; Wang, X.; Huang, P. Y.; Cahill, D. G.; Lv, B. High thermal conductivity in cubic boron arsenide crystals. *Science* **2018**, *361*, 579–581.
[122] Kang, J. S.; Li, M.; Wu, H.; Nguyen, H.; Hu, Y. Experimental observation of high thermal conductivity in boron arsenide. *Science* **2018**, *361*, 575–578.
[123] Tian, F.; Song, B.; Chen, X.; Ravichandran, N. K.; Lv, Y.; Chen, K.; Sullivan, S.; Kim, J.; Zhou, Y.; Liu, T.-H. et al. Unusual high thermal conductivity in boron arsenide bulk crystals. *Science* **2018**, *361*, 582–585.
[124] Li, S.; Qin, Z.; Wu, H.; Li, M.; Kunz, M.; Alatas, A.; Kavner, A.; Hu, Y. Anomalous thermal transport under high pressure in boron arsenide. *Nature* **2022**, *612*, 459–464.
[125] Ravichandran, N. K.; Broido, D. Non-monotonic pressure dependence of the thermal conductivity of boron arsenide. *Nat. Commun.* **2019**, *10*, 827.
[126] Meng, X.; Singh, A.; Juneja, R.; Zhang, Y.; Tian, F.; Ren, Z.; Singh, A. K.; Shi, L.; Lin, J. F.; Wang, Y. Pressure-dependent behavior of defect-modulated band structure in boron arsenide. *Adv. Mater.* **2020**, *32*, e2001942.
[127] Song, T.; Fei, Z.; Yankowitz, M.; Lin, Z.; Jiang, Q.; Hwangbo, K.; Zhang, Q.; Sun, B.; Taniguchi, T.; Watanabe, K. et al. Switching 2D magnetic states via pressure tuning of layer stacking. *Nat. Mater.* **2019**, *18*, 1298–1302.
[128] Burch, K. S.; Mandrus, D.; Park, J. G. Magnetism in two-dimensional van der Waals materials. *Nature* **2018**, *563*, 47–52.
[129] Li, T.; Jiang, S.; Sivadas, N.; Wang, Z.; Xu, Y.; Weber, D.; Goldberger, J. E.; Watanabe, K.; Taniguchi, T.; Fennie, C. J.; Mak, K. F.; Shan, J. Pressure-controlled interlayer magnetism in atomically thin CrI_3. *Nat. Mater.* **2019**, *18*, 1303–1308.
[130] Hsieh, S.; Bhattacharyya, P.; Zu, C.; Mittiga, T.; Smart, T. J.; Machado, F.; Kobrin, B.; Höhn, T. O.; Rui, N. Z.; Kamrani, M. et al. Imaging stress and magnetism at high pressures using a nanoscale quantum sensor. *Science* **2019**, *366*, 1349–1354.
[131] Lesik, M.; Plisson, T.; Toraille, L.; Renaud, J.; Occelli, F.; Schmidt, M.; Salord, O.; Delobbe, A.; Debuisschert, T.; Rondin, L. et al. Magnetic measurements on micrometer-sized samples under high pressure using designed NV centers. *Science* **2019**, *366*, 1359–1362.
[132] Yip, K. Y.; Ho, K. O.; Yu, K. Y.; Chen, Y.; Zhang, W.; Kasahara, S.; Mizukami, Y.; Shibauchi, T.; Matsuda, Y.; Goh, S. K. et al. Measuring magnetic field texture in correlated electron systems under extreme conditions. *Science* **2019**, *366*, 1355–1359.
[133] Ishizuka, M.; Yamada, I.; Amaya, K.; Endo, S. Change of magnetism in the two-dimensional Heisenberg ferromagnet K_2CuF_4 observed at high pressures. *J. Phys. Soc. Jpn* **1996**, *65*, 1927–1929.
[134] Martins, L. G. P.; Matos, M. J. S.; Paschoal, A. R.; Freire, P. T. C.; Andrade, N. F.; Aguiar, A. L.; Kong, J.; Neves, B. R. A.; de Oliveira, A. B.; Mazzoni, M. S. C.; Filho, A. G. S.; Cancado, L. G. Raman evidence for pressure-induced formation of diamondene. *Nat. Commun.* **2017**, *8*, 96.
[135] Barboza, A. P.; Guimaraes, M. H.; Massote, D. V.; Campos, L. C.; Barbosa Neto, N. M.; Cancado, L. G.; Lacerda, R. G.; Chacham, H.; Mazzoni, M. S.; Neves, B. R. Room-temperature compression-induced diamondization of few-layer graphene. *Adv. Mater.* **2011**, *23*, 3014–3017.
[136] Mao, W. L.; Mao, H. K.; Eng, P. J.; Trainor, T. P.; Newville, M.; Kao, C. C.; Heinz, D. L.; Shu, J.; Meng, Y.; Hemley, R. J. Bonding changes in compressed superhard graphite. *Science* **2003**, *302*, 425–427.
[137] Yu, Z.; Xia, W.; Xu, K.; Xu, M.; Wang, H.; Wang, X.; Yu, N.; Zou, Z.; Zhao, J.; Wang, L. et al. Pressure-induced structural phase transition and a special amorphization phase of two-dimensional ferromagnetic semiconductor $Cr_2Ge_2Te_6$. *J. Phys. Chem. C* **2019**, *123*, 13885–13891.
[138] Chen, L.-C.; Chen, P.-Q.; Li, W.-J.; Zhang, Q.; Struzhkin, V. V.; Goncharov, A. F.; Ren, Z.; Chen, X.-J. Enhancement of thermoelectric performance across the topological phase transition

in dense lead selenide. *Nat. Mater.* **2019**, *18*, 1321–1326.
[139] Chen, L.-C.; Yu, H.; Pang, H.-J.; Jiang, B.-B.; Su, L.; Shi, X.; Chen, L.-D.; Chen, X.-J. Pressure-induced enhancement of thermoelectric performance in palladium sulfide. *Mater. Tod. Phys.* **2018**, *5*, 64–71.
[140] Yu, H.; Chen, L.-C.; Pang, H.-J.; Qin, X.-Y.; Qiu, P.-F.; Shi, X.; Chen, L.-D.; Chen, X.-J. Large enhancement of thermoelectric performance in $CuInTe_2$ upon compression. *Mater. Tod. Phys.* **2018**, *5*, 1–6.
[141] Baker, J. L.; Kumar, R. S.; Park, C.; Velisavljevic, N.; Cornelius, A. Compressibility and thermoelectric behavior of TiCoSb half-Heusler compound at high pressures. *Intermetallics* **2018**, *95*, 137–143.
[142] Pang, H.-J.; Yu, H.; Chen, L.-C.; Fu, C.-G.; Zhu, T.-J.; Chen, X.-J. Pressure tuning of thermoelectric performance in FeNbSb. *J. Alloy. Compd.* **2019**, *805*, 1224–1230.

Zhen Wu is currently a research scientist at College of Engineering and Applied Science, Nanjing University. He received his B.S. degree in applied chemistry from Shandong University in 2010 and his Ph.D. in inorganic chemistry from Shandong University in 2017. His research interests include 2D materials, high pressure science and thermal management.

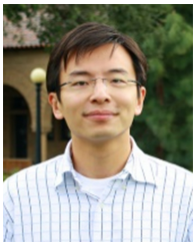

Jia Zhu is a professor at College of Engineering and Applied Science, Nanjing University. He received his M.S. at Nanjing University and Ph.D. in electrical engineering from Stanford University. He worked as a postdoctoral fellow at University of California, Berkeley and Lawrence Berkeley National Lab. His research interest is in the area of nanomaterials, nanophotonics, and nanoscale heat transfer.